[28] J. I. Steinfeld, *Molecules and Radiation: an Introduction to Modern Molecular Spectroscopy* (Dover, New York, 1985)

[29] H. Lefebvre-Brion, and R. W. Field, *Perturbations in the Spectra of Diatomic Molecules* (Academic Press, Orlando, 1986)

[30] X. Xie, and R. W. Field, Chem. Phys. **99**, 337 (1985)

[31] L. Morgus, Ph.D. Thesis, Lehigh University (2005)

[32] L. Veseth, Theo. Chim. Acta, **18**, 368 (1970)

[33] R. N. Zare, *Angular Momentum*, Wiley-Interscience, New York, 1986

[34] M. Blume, A. J. Freeman, and R. E. Watson, Phys Rev. A, **134**, 320 (1964)

[35] W.-H. Jeng, X. Xie, L. P. Gold, and R. A. Bernheim, J. Chem. Phys. **94**, 928 (1991)

[36] K. Kayama, and J. C. Baird, J. Chem. Phys., **46**, 2604 (1967)

[37] G. Herzberg, *Molecular Spectra and Molecular Structure I, Spectra of Diatomic Molecules*, D. Van Nostrand Company Inc., Princeton (1950)

[38] H. Sun, and J. Huennekens, J. Chem. Phys., **97**, 4714 (1992)

[39] D. L. Cooper, J. M. Hutson, and T. Uzer, Chem. Phys. Lett., **86**, 472 (1982)

[40] G. Lazarov, A. M. Lyyra, and L. Li, J. Mol. Spectroscopy, **205**, 73 (2001)

[41] P. Yi, B. Ji, A. S.-C. Cheung, W. C. Stwalley, R. W. Field, A. M. Lyyra, and L. Li, Chem. Phys. Lett. **349**, 426 (2002)

[42] T. Kirova, PhD. Thesis, Temple University (2005)

[43] T. Kirova, and F. C. Spano, Phys. Rev. A **71**, 063816 (2005)

[44] P. R. Berman. Phys. Rev. A **58**, 4886 (1998)

[45] F. C. Spano, J. Chem. Phys. **114**, 276 (2001)

CHAPTER 4

DENSITY MATRIX FORMALISM

4.1 Introduction

Several theoretical methods have been developed to model the interaction of light with matter. In this chapter, we introduce a model to simulate our experimental data that is based on the density matrix equations of motion developed by J. von Neumann in 1927. In this method, the atom is treated quantum mechanically, while the electromagnetic fields of each laser are treated semi-classically. Such treatment makes the approach easier to visualize and not as abstract as a pure quantum mechanical treatment. This method utilizes a statistical average approach to model an ensemble of quantum systems. Another desirable feature of this approach is the inclusion of relaxation terms, such as spontaneous decay, collisional effects, and other decoherence phenomena that give rise to broadening in linewidths. Since these key physical processes are included in this model, the density matrix approach is an excellent method to simulate our experimental data.

4.2 The Density Matrix

Our system can be represented by an ensemble of atoms in given quantum mechanical states. Any pure quantum mechanical state can be described by a wave function, ψ_k, from which all observable information about the state can be extracted. Such wave functions must satisfy the well known Schrodinger equation

$$i\hbar \frac{d\psi_k}{dt} = \hat{H}\psi_k \tag{4.1}$$

where $\hat{H}$ is the Hamiltonian operator of the system. In our case, the atoms occupy mixed states for which the exact wavefunctions cannot be known. Each pure state ψ_k, however, can be expanded in an orthonormal basis set of the energy eigenvectors of the unperturbed Hamiltonian $|\phi_i>$, which satisfy the condition

$$\int \phi_n^{*}(\vec{r})\phi_m(\vec{r})dr^3 = \delta_{nm}. \tag{4.2}$$

Therefore, our pure state can be written in the form

$$\psi_k(\vec{r},t) = \sum_{i=1}^{N} c_i(t) \,|\, \phi_i(\vec{r}) > \tag{4.3}$$

where the sum is over the total N energy eigenstates of the system, and the coefficients c_i, define the probability amplitude of finding a system in state $|\phi_i>$ at a time t, and satisfy the condition

$$\sum_{i=1}^{N} |\, c_i(t) \,|^2 = 1. \tag{4.4}$$

Since the wavefunctions of these pure states form a complete set, our mixed state can be written as a superposition of these pure states, with statistical weights p_k, which indicate the probability of finding the system in a state ψ_k, and which satisfies the condition

$$\sum_k p_k = 1. \tag{4.5}$$

The expectation value of an operator $\hat{O}$ for a system in a pure state can be expressed as

$$< \hat{O} > = < \psi_k \,|\, \hat{O} \,|\, \psi_k > = \sum_{m,n} c_m^{*} c_n O_{mn} \tag{4.6}$$

with O_{mn} being the matrix representation of $\hat{O}$ defined by

$$O_{mn} = \int u^*_m(\vec{r})\hat{O}u_n(\vec{r})dr^3 . \tag{4.7}$$

The specific operator necessary for our case is the density operator. The density operator of a pure state is defined as [1-3]

$$\hat{\rho} = |\psi_k><\psi_k| \tag{4.8}$$

and can be represented as an N x N matrix. The elements of the matrix are written as

$$\rho_{nm} = <\phi_n|\rho|\phi_m> = <\phi_n|\psi_k><\psi_k|\phi_m> = c_n c^*_m . \tag{4.9}$$

Therefore, the expression for our expectation value in a pure system (equation 4.6) can now be written as

$$<\hat{O}> = \sum_{m,n} \rho_{nm} O_{mn} = \sum_n (\rho O)_{nn} = Tr(\hat{\rho}\hat{O}) \tag{4.10}$$

If we use the identity operator in the above equation, we find

$$Tr(\hat{\rho}\hat{1}) = \sum_{i=1}^{n} \rho_{ii} = 1 \tag{4.11}$$

which is the trace normalization property. This can be rewritten as

$$\rho_{11} = 1 - \sum_{i=2}^{n} \rho_{ii} \tag{4.12}$$

Using the above relation we can eliminate one degree of freedom in our system, thus reducing the number of equations that have to be solved.

Since our system is an ensemble of molecules, we need to use the average value of the expectation value of an operator. The average value of an operator in an ensemble is defined as

$$< \hat{O} >= \sum_k p_k < \hat{O} >_k = \sum_k p_k < \psi_k \mid \hat{O} \mid \psi_k > = \sum_k p_k \sum_{mn} c_m^* c_n O_{mn} . \quad (4.13)$$

Therefore the density operator for our mixed states is then [3, 4]

$$\hat{\rho} = \sum_k p_k \mid \psi_k >< \psi_k \mid \quad (4.14)$$

whose individual elements have the form

$$\rho_{nm} = \sum_k p_k c_m^* c_n . \quad (4.15)$$

Once the density matrix for a given system is known, any observable of that system can then be found. Diagonal elements of the density matrix, ρ_{nn}, give the probability of finding the system in the n^{th} state, and therefore indicate the population of that state. Off diagonal elements of the density matrix, ρ_{mn}, represent the coherences between states m and n since they involve the phase differences between c_m and c_n [5]. Hence, off diagonal elements vanish for incoherent processes. The coherences can be broken up into real and imaginary parts. The real part of the expression corresponds to the dispersion of the system and the imaginary part corresponds to the absorption between states "m" and "n".

The density matrix equations of motion can now be derived. First, we take the time derivative of the density operator

$$\dot{\hat{\rho}} = \sum_k p_k \mid \dot{\psi}_k >< \psi_k \mid + \sum_k p_k \mid \psi_k >< \dot{\psi}_k \mid . \quad (4.16)$$

Using the Schrodinger equation, this expression can be rewritten as

$$\dot{\hat{\rho}} = -\frac{i}{\hbar} \sum_k p_k \hat{H} \mid \psi_k >< \psi_k \mid + \frac{i}{\hbar} \sum_k p_k \mid \psi_k >< \psi_k \mid \hat{H} . \quad (4.17)$$

Since the p_k are statistical weights (i.e. just numbers), our equation becomes

$$\dot{\hat{\rho}} = -\frac{i}{\hbar}\hat{H}\hat{\rho} + \frac{i}{\hbar}\hat{\rho}\hat{H} \ . \tag{4.18}$$

Using the definition for the commutator $[\hat{H}, \hat{\rho}] = \hat{H}\hat{\rho} - \hat{\rho}\hat{H}$, we then arrive at

$$\dot{\hat{\rho}} = -\frac{i}{\hbar}[\hat{H}, \hat{\rho}], \tag{4.19}$$

which is the Liouville equation, or the density matrix equations of motion.

The equation of motion for a given element of the matrix is written as

$$\dot{\rho}_{nm} = -\frac{i}{\hbar}[\hat{H}, \hat{\rho}]_{nm} = -\frac{i}{\hbar}(\hat{H}\hat{\rho} - \hat{\rho}\hat{H})_{nm} = -\frac{i}{\hbar} < n \mid \hat{H}\hat{\rho} - \hat{\rho}\hat{H} \mid m > . \tag{4.20}$$

Noting that $\sum_{k=1} \mid k >< k \mid = 1$, we can insert this expression into the above equation,

which then becomes

$$\dot{\rho}_{nm} = -\frac{i}{\hbar}\sum_{k=1}[< n \mid \hat{H} \mid k >< k \mid \hat{\rho} \mid m > - < n \mid \hat{\rho} \mid k >< k \mid \hat{H} \mid m >], \tag{4.21}$$

$$\dot{\rho}_{nm} = \sum_{k=1}(H_{nk}\rho_{km} - \rho_{nk}H_{km}) \ . \tag{4.22}$$

This is a commonly used form for the density matrix equations of motion.

The complete Hamiltonian of our molecule-laser system consists of three parts: the Hamiltonian of the unperturbed molecule H_{mol}, the spin-orbit perturbation V^{SO} between the mixed states, and the interaction of the molecule with the electric field H_{int}. Therefore, the Hamiltonian of our system can be written as

$$H = H_{mol} + V^{SO} + H_{\text{int}} . \tag{4.23}$$

We will write the molecular Hamiltonian as the sum of two parts [3], one involving the laser frequencies, H_0 , and one involving the detunings, H_1

$$H_{mol} = H_0 + H_1, \tag{4.24}$$

which will allow us to use the rotating wave approximation for our rapidly oscillating fields. This gives the full expression for our Hamiltonian as

$$H = H_0 + H_1 + V^{SO} + H_{\text{int}}. \tag{4.25}$$

Substituting this into the density matrix equations of motion described above gives

$$\frac{d\rho}{dt} = -\frac{i}{\hbar}[H_0 + H_1 + V^{SO} + H_{\text{int}}, \rho]. \tag{4.26}$$

To model our system in the interaction picture, which involves the interaction of the molecule with the laser light, we will impose a unitary transformation of the form [1]

$$\rho_I = e^{\frac{iH_0 t}{\hbar}} \rho e^{\frac{-iH_0 t}{\hbar}}. \tag{4.27}$$

Differentiating the above expression with respect to time gives

$$\frac{d\rho_I}{dt} = \frac{i}{\hbar} e^{\frac{iH_0 t}{\hbar}} [H_0, \rho_I] e^{\frac{-iH_0 t}{\hbar}} + e^{\frac{iH_0 t}{\hbar}} \frac{d\rho}{dt} e^{\frac{-iH_0 t}{\hbar}}. \tag{4.28}$$

Substituting $\frac{d\rho}{dt}$ from equation (4.26) into equation (4.28) results in the more simplified form

$$\frac{d\rho_I}{dt} = -\frac{i}{\hbar} e^{\frac{iH_0 t}{\hbar}} [H_1 + V^{SO} + H_{\text{int}}, \rho_I] e^{\frac{-iH_0 t}{\hbar}}. \tag{4.29}$$

The Hamiltonian in the interaction picture is obtained through another unitary transformation, namely

$$H_I = e^{\frac{iH_0 t}{\hbar}} (H_1 + V^{SO} + H_{\text{int}}) e^{\frac{-iH_0 t}{\hbar}} \tag{4.30}$$

which we will use in section 4.5 to obtain the density matrix equations of motion in the interaction picture

$$\frac{d\rho_I}{dt} = -\frac{i}{\hbar}[H_I, \rho_I]. \tag{4.31}$$

4.3 Decay Terms

Equation (4.31) only includes the interaction of the optical fields with the molecule. To accurately describe our system, all decay phenomena (spontaneous emission, collisions, transit time of molecules through the laser beam, etc.) must also be included in the density matrix expressions

$$\dot{\rho}_{nm} = -\frac{i}{\hbar}[\hat{H}, \hat{\rho}]_{nm} + \textit{ relaxation terms.} \tag{4.32}$$

All of these relaxation terms are collectively expressed by an N x N matrix $\Gamma(\rho)$

$$\Gamma(\rho) = \delta_{nm}(-W_n\rho_{nm} + \sum_{\substack{k=2 \\ k\neq i}} \Theta(\varepsilon_k - \varepsilon_n)W_{kn}\rho_{kk}) - (1-\delta_{nm})\gamma_{nm}\rho_{nm}. \tag{4.33}$$

A level "n" can spontaneously emit a photon to all lower energy levels to which electric dipole transitions are allowed. We denote the total radiative decay rate from level n as W_n, defined as

$$W_n = \sum_{m=1}^{N} W_{nm} \tag{4.34}$$

where W_{nm} is the rate of decay between levels n and m, and the sum is over the total number of levels in the system lower than level n. Spontaneous emission directly affects the population of a given level, and therefore involves the elements ρ_{nn}. Typical radiative decay rates are of the order of ~50 rad/s for levels with lifetimes of ~20ns. To account

for the fact that the molecules are traveling in and out of the laser beam, the beam transit rate, w_t, is included for levels with long lifetimes [6, 7]. The expression for the transit rate is found to be [7]

$$w_t = 0.962 \frac{u_{rms}}{r_{1/e^2}} \tag{4.35}$$

where the root mean square velocity of the molecules is $u_{rms} = \sqrt{\frac{3RT}{M}}$ (where R is the gas constant, T is the temperature in Kelvin, and M is the molar mass in kg), and r_{1/e^2} is the distance from the center of the laser beam to where the intensity drops to $1/e^2$ of its peak value. Since the temperature for our experiment was around 855K, the values used to calculate w_t were u_{rms} =1240m/s, and r_{1/e^2} =100 – 250 μ m, giving a transit rate range of 30 – 75 rad/s. An additional positive term, which we denote as λ, must be added to the ground state equation of motion ($\dot{\rho}_{11}$) to account for new molecules entering the path of the laser beam.

The off diagonal elements of $\Gamma(\rho)$ include the phenomenological dephasing parameters γ_{ij}. These terms account for the processes that prevent the natural inclination of the system toward equilibrium and are commonly expressed as [8, 9]

$$\gamma_{nm} = \frac{1}{2} \sum_{k=1,5} (W_{nk} + W_{mk}) + \gamma^c{}_{nm} \quad . \qquad n \neq m \tag{4.36}$$

The term $\gamma^c{}_{nm}$ includes the dephasing effects from collisions of the atoms or molecules. A diagram of all possible decay channels for our five level experiment is displayed in Figure 4.1.

To summarize the form for all relaxation terms that must be included in each element of the equations of motion:

$$\dot{\rho}_{nn} = \ldots - (W_n + w_t)\rho_{nn} + \sum_{m>n} W_{mn}\rho_{mm} \qquad \text{diagonal elements}$$

$$\dot{\rho}_{nm} = \ldots - (\gamma_{nm} + w_t)\rho_{nm} \qquad \text{off-diagonal elements} \qquad (4.37)$$

$$\dot{\rho}_{11} = \ldots - w_t\rho_{11} + \lambda \qquad \text{ground state}$$

Since we now know the form of all terms in the density matrix equations of motion,

$$\dot{\rho}_{nm} = -\frac{i}{\hbar}[\hat{H}, \hat{\rho}]_{nm} + \Gamma(\rho) \qquad (4.38)$$

we can proceed to find the exact form of the expressions for our system.

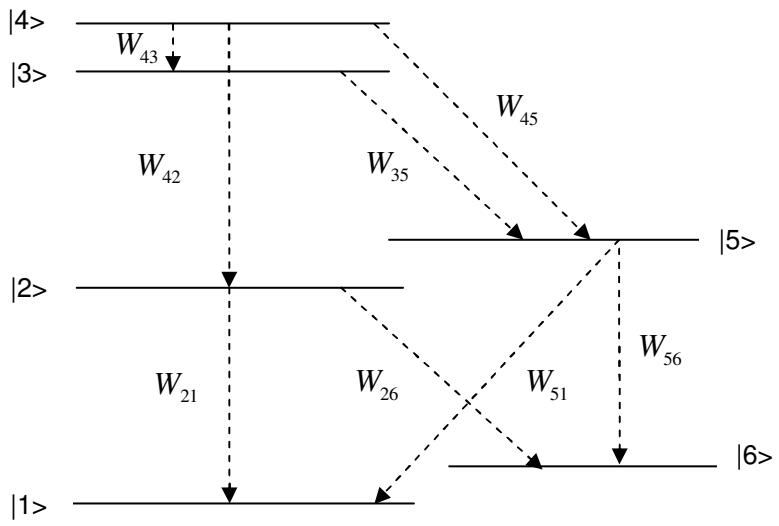

Figure 4.1 Spontaneous decay channels between all levels involved in our excitation scheme. Level |6> represents all other ground state levels to which the other levels may decay.

4.4 Energy Scheme

The five-level energy level scheme involving three lasers used in this analysis is displayed in Figure 4.2. Levels 1 and 2 are the ground and intermediate states in our excitation scheme, respectively. Levels 3 and 4 represent the unperturbed triplet and singlet states of our spin-orbit mixed levels, respectively. The coupling field connects Level 4 with a second intermediate Level 5. The unperturbed energy separation between the upper singlet and triplet states is denoted by Δ_0. The frequency of the lasers are represented by ω_{L_i}, and the Rabi frequency between levels "*i*" and "*j*" is shown in the diagram as Ω_{ij}.

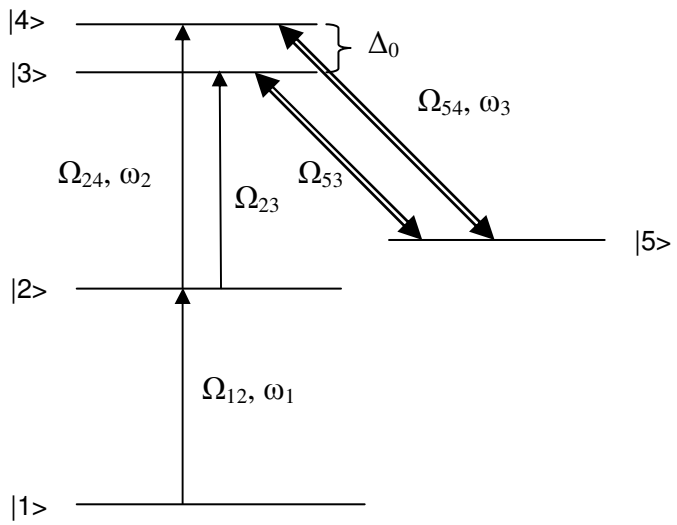

Figure 4.2 Excitation scheme of a five-level molecular system interacting with three laser fields. Ω_{ij} indicates the Rabi frequency between levels *i* and *j*. The laser field frequency is indicated by ω_i. Δ_0 is the unperturbed energy separation between the upper singlet and triplet states.

4.5 Deriving the Hamiltonian

As previously mentioned, the Hamiltonian for our system can be expressed as

$$H = H_{mol} + V^{so} + H_{\text{int}} \quad \text{or} \quad H = H_0 + H_1 + V^{so} + H_{\text{int}}. \tag{4.39}$$

For an *N* level system, the molecular Hamiltonian of the unperturbed molecule is diagonal in the basis set of the molecular states $|k\rangle$, and can simply be expressed as

$$H_{mol} = \sum_{k=1}^{N} \varepsilon_k \, |k\rangle\langle k| \tag{4.40}$$

The eigenvalues of the molecular Hamiltonian, ε_k, are the energies of the k^{th} level. Therefore, by setting $\varepsilon_1=0$, our five-level system unperturbed molecular Hamiltonian is expressed as

$$H_{mol} = \varepsilon_2 |2\rangle\langle 2| + \varepsilon_3 |3\rangle\langle 3| + \varepsilon_4 |4\rangle\langle 4| + \varepsilon_5 |5\rangle\langle 5| \quad . \tag{4.41}$$

Dividing the molecular Hamiltonian into two parts, we define H_0

$$\begin{aligned} H_0 = {} & \hbar\omega_1 |2\rangle\langle 2| + (\hbar\omega_1 + \hbar\omega_2) |3\rangle\langle 3| + (\hbar\omega_1 + \hbar\omega_2) |4\rangle\langle 4| + \\ & (\hbar\omega_1 + \hbar\omega_2 - \hbar\omega_3) |5\rangle\langle 5| \end{aligned} \tag{4.42}$$

and H_1, which involves the detunings of the optical fields,

$$\begin{aligned} H_1 = {} & -(\hbar\omega_1 - \varepsilon_2) |2\rangle\langle 2| - (\hbar\omega_1 + \hbar\omega_2 - \varepsilon_3) |3\rangle\langle 3| - \\ & (\hbar\omega_1 + \hbar\omega_2 - \varepsilon_4) |4\rangle\langle 4| - (\hbar\omega_1 + \hbar\omega_2 - \hbar\omega_3 - \varepsilon_5) |5\rangle\langle 5|. \end{aligned} \tag{4.43}$$

The perturbation V^{SO} can be written as

$$V^{so} = \hbar V (|4\rangle\langle 3| + |3\rangle\langle 4|) \tag{4.44}$$

where *V* is the spin-orbit interaction defined by equation (3.35). Using the dipole approximation, the interaction Hamiltonian is generally defined as [1, 2]

$$H_{\text{int}} = -e\vec{r}\cdot\vec{E} = -\vec{\mu}\cdot\vec{E} \tag{4.45}$$

where $\vec{\mu}$ is the dipole moment operator, and $\vec{E}$ is the electric field of the applied laser. The electric field of each laser is written in the form

$$\vec{E}(t) = E_0\,\hat{e}\cos(\omega t) \tag{4.46}$$

where E_0 is the electric field amplitude, ω is the frequency of the incident radiation, t is the time elapsed, and $\hat{e}$ is the direction of polarization. The Rabi frequencies, as discussed in section 2.9, corresponding to each transition, are defined as

$$\Omega_{12} = \frac{\mu_{12}E_1}{\hbar}, \Omega_{23} = \frac{\mu_{23}E_2}{\hbar}, \Omega_{24} = \frac{\mu_{24}E_2}{\hbar}, \Omega_{53} = \frac{\mu_{53}E_3}{\hbar}, \Omega_{54} = \frac{\mu_{54}E_3}{\hbar} \tag{4.47}$$

Therefore, the interaction term of the Hamiltonian, which involves off diagonal elements, can be written as

$$\begin{aligned} H_{\text{int}} = {} & \hbar\frac{\Omega_{12}}{2}[|2><1|+|1><2|][e^{-i\omega_1 t}+e^{i\omega_1 t}] + \hbar\frac{\Omega_{23}}{2}[|3><2|+|2><3|][e^{-i\omega_2 t}+e^{i\omega_2 t}] + \\ & \hbar\frac{\Omega_{24}}{2}[|4><2|+|2><4|][e^{-i\omega_2 t}+e^{i\omega_2 t}] + \hbar\frac{\Omega_{53}}{2}[|5><3|+|3><5|][e^{-i\omega_3 t}+e^{i\omega_3 t}] + \\ & \hbar\frac{\Omega_{54}}{2}[|5><4|+|4><5|][e^{-i\omega_3 t}+e^{-i\omega_3 t}]. \end{aligned} \tag{4.48}$$

Performing the unitary transformation of (4.30) will give us the Hamiltonian in the interaction picture for our system. Since our system oscillates at a frequency much smaller than the frequency of our resonant optical fields, we can employ the rotating wave approximation [10] and obtain a much simplified expression for H_I, namely

$$H_I = -\hbar\Delta_1 |2\rangle\langle 2| - \hbar(\Delta_1 + \Delta_2)|3\rangle\langle 3| - \hbar(\Delta_1 + \Delta_2 - \Delta_0)|4\rangle\langle 4| -$$
$$\hbar(\Delta_1 + \Delta_2 - \Delta_3 - \Delta_0)|5\rangle\langle 5| + \hbar V(|4\rangle\langle 3| + |3\rangle\langle 4|) + \hbar\frac{\Omega_{12}}{2}(|2\rangle\langle 1| + |1\rangle\langle 2|) +$$
$$+\hbar\frac{\Omega_{23}}{2}(|3\rangle\langle 2| + |2\rangle\langle 3|) + \hbar\frac{\Omega_{24}}{2}(|4\rangle\langle 2| + |2\rangle\langle 4|) + \hbar\frac{\Omega_{53}}{2}(|5\rangle\langle 3| + |3\rangle\langle 5|) \quad (4.49)$$
$$+\hbar\frac{\Omega_{54}}{2}(|5\rangle\langle 4| + |4\rangle\langle 5|)$$

where the detunings of each laser are defined as

$$\Delta_1 = \omega_1 - \frac{\varepsilon_2}{\hbar},\ \Delta_2 = \omega_2 - \frac{\varepsilon_3 - \varepsilon_2}{\hbar},\ \Delta_3 = \omega_3 - \frac{\varepsilon_4 - \varepsilon_5}{\hbar} \quad (4.50)$$

and the energy difference between the two unperturbed states is

$$\Delta_0 = \frac{\varepsilon_4 - \varepsilon_3}{\hbar} \quad . \quad (4.51)$$

To account for the slight effect of Doppler broadening upon our system, we introduce a velocity-dependent detuning for each laser. The pump laser L_1 co-propagates with the coupling field L_3, while the probe field L_2 counter-propagates to both L_1 and L_3. Molecules traveling along the propagation direction will experience a smaller frequency than the actual frequency of the laser, therefore the laser detunings in the molecule frame of reference are defined as

$$\delta_1 \equiv \Delta_1 - k_1 v_z,\ \delta_2 \equiv \Delta_2 + k_2 v_z,\ \ \delta_3 \equiv \Delta_3 - k_3 v_z \quad (4.52)$$

where k_i is the wave number of laser "*i*" whose beam has a propagation axis *z*, and v_z is the *z*-component of the velocity of the molecule. This gives the final Hamiltonian in the interaction picture the form

$$H_I = -\hbar\delta_1 |2><2| -\hbar(\delta_1+\delta_2)|3><3| -\hbar(\delta_1+\delta_2-\Delta_0)|4><4| -\hbar(\delta_1+\delta_2-\delta_3-\Delta_0)|5><5| +$$
$$\hbar V(|4><3|+|3><4|)+\hbar\frac{\Omega_{12}}{2}(|2><1|+|1><2|)+\hbar\frac{\Omega_{23}}{2}(|3><2|+|2><3|)+ \quad (4.53)$$
$$\hbar\frac{\Omega_{24}}{2}(|4><2|+|2><4|)+\hbar\frac{\Omega_{53}}{2}(|5><3|+|3><5|)+\hbar\frac{\Omega_{54}}{2}(|5><4|+|4><5|).$$

Now that we have our Hamiltonian in the interaction picture, we can substitute it into the interaction picture density matrix equations of motion

$$\frac{d\rho_I}{dt} = -\frac{i}{\hbar}[H_I, \rho_I] \ + \text{relaxation terms}$$

and obtain the individual elements of the density matrix with all pertinent relaxation terms. The density matrix equations with all included relaxation terms are listed below. All equations were checked for correctness against Ref. [11].

$$\dot{\rho}_{11} = -i\frac{\Omega_{12}}{2}\rho_{21} + i\frac{\Omega_{12}}{2}\rho_{12} + W_{21}\rho_{22} + W_{31}\rho_{33} + W_{41}\rho_{44} + W_{51}\rho_{55} - w_t\rho_{11} + \lambda \quad (4.54a)$$

$$\dot{\rho}_{12} = -i\frac{\Omega_{12}}{2}\rho_{22} + i\frac{\Omega_{12}}{2}\rho_{11} + i\frac{\Omega_{23}}{2}\rho_{13} + i\frac{\Omega_{24}}{2}\rho_{14} - (\gamma_{12} + i\delta_1 + w_t)\rho_{12} \quad (4.54b)$$

$$\dot{\rho}_{13} = -i\frac{\Omega_{12}}{2}\rho_{23} + i\frac{\Omega_{23}}{2}\rho_{12} - (i\delta_1 + i\delta_2 + w_t + \gamma_{13})\rho_{13} + iV\rho_{14} + i\frac{\Omega_{53}}{2}\rho_{15} \quad (4.54c)$$

$$\dot{\rho}_{14} = -i\frac{\Omega_{12}}{2}\rho_{24} + i\frac{\Omega_{24}}{2}\rho_{12} - (i\delta_1 + i\delta_2 - i\Delta_0 + w_t)\rho_{14} + iV\rho_{13} + i\frac{\Omega_{54}}{2}\rho_{15} - \gamma_{14}\rho_{14} \quad (4.54d)$$

$$\dot{\rho}_{15} = -i\frac{\Omega_{12}}{2}\rho_{25} + i\frac{\Omega_{53}}{2}\rho_{13} - (i\delta_1 + i\delta_2 - i\delta_3 - i\Delta_0 + w_t)\rho_{15} + i\frac{\Omega_{54}}{2}\rho_{14} - \gamma_{15}\rho_{15} \quad (4.54e)$$

$$\dot{\rho}_{21} = \dot{\rho}_{12}^{\ *} \quad (4.54f)$$

$$\dot{\rho}_{22} = -i\frac{\Omega_{12}}{2}\rho_{12} - i\frac{\Omega_{23}}{2}\rho_{32} - i\frac{\Omega_{24}}{2}\rho_{42} + i\frac{\Omega_{12}}{2}\rho_{21} + i\frac{\Omega_{23}}{2}\rho_{23} + i\frac{\Omega_{24}}{2}\rho_{24} + \quad (4.54g)$$
$$+ W_{42}\rho_{44} + W_{32}\rho_{33} + W_{52}\rho_{55} - (W_{21} + w_t)\rho_{22}$$

$$\dot{\rho}_{23} = -i\frac{\Omega_{12}}{2}\rho_{13} - (i\delta_2 + w_t)\rho_{23} - i\frac{\Omega_{23}}{2}\rho_{33} - i\frac{\Omega_{24}}{2}\rho_{43} + i\frac{\Omega_{23}}{2}\rho_{22} + \tag{4.54h}$$

$$+ i\frac{\Omega_{34}}{2}\rho_{24} + i\frac{\Omega_{53}}{2}\rho_{25} - \gamma_{23}\rho_{23}$$

$$\dot{\rho}_{24} = -i\frac{\Omega_{12}}{2}\rho_{14} - i\frac{\Omega_{23}}{2}\rho_{34} - i\frac{\Omega_{24}}{2}\rho_{44} + i\frac{\Omega_{24}}{2}\rho_{22} + iV\rho_{23} + i\frac{\Omega_{54}}{2}\rho_{25} \tag{4.54i}$$

$$-(i\delta_2 - i\Delta_0 + \gamma_{24} + w_t)\rho_{24}$$

$$\dot{\rho}_{25} = -i\frac{\Omega_{12}}{2}\rho_{15} - i\frac{\Omega_{23}}{2}\rho_{35} + i\frac{\Omega_{53}}{2}\rho_{23} - i\frac{\Omega_{24}}{2}\rho_{45} - (i\delta_2 - i\delta_3 - i\Delta_0 + w_t)\rho_{25} + \tag{4.54j}$$

$$+ i\frac{\Omega_{53}}{2}\rho_{23} + i\frac{\Omega_{54}}{2}\rho_{24} - \gamma_{25}\rho_{25}$$

$$\dot{\rho}_{31} = \dot{\rho}_{13}^{\ *} \tag{4.54k}$$

$$\dot{\rho}_{32} = \dot{\rho}_{23}^{\ *} \tag{4.54l}$$

$$\dot{\rho}_{33} = -i\frac{\Omega_{23}}{2}\rho_{23} - iV\rho_{43} - i\frac{\Omega_{53}}{2}\rho_{53} + i\frac{\Omega_{23}}{2}\rho_{32} + iV\rho_{34} + i\frac{\Omega_{53}}{2}\rho_{35} + \rho_{33} + \tag{4.54m}$$

$$+ W_{43}\rho_{44} - (W_3 + w_t)\rho_{33}$$

$$\dot{\rho}_{34} = -i\frac{\Omega_{23}}{2}\rho_{24} - iV\rho_{44} - i\frac{\Omega_{53}}{2}\rho_{54} + i\frac{\Omega_{24}}{2}\rho_{32} + iV\rho_{33} + i\frac{\Omega_{54}}{2}\rho_{35} \tag{4.54n}$$

$$+ i\Delta_0\rho_{34} - (\gamma_{34} + w_t)\rho_{34}$$

$$\dot{\rho}_{35} = -i\frac{\Omega_{23}}{2}\rho_{25} - iV\rho_{45} - i\frac{\Omega_{53}}{2}\rho_{55} + i\frac{\Omega_{53}}{2}\rho_{33} + i\frac{\Omega_{54}}{2}\rho_{34} \tag{4.54o}$$

$$+ (i\Delta_0 + i\delta_3 - w_t - \gamma_{35})\rho_{35}$$

$$\dot{\rho}_{41} = \dot{\rho}_{14}^{\ *} \tag{4.54p}$$

$$\dot{\rho}_{42} = \dot{\rho}_{24}^{\ *} \tag{4.54q}$$

$$\dot{\rho}_{43} = \dot{\rho}_{34}^{*} \tag{4.54r}$$

$$\dot{\rho}_{44} = -i\frac{\Omega_{24}}{2}\rho_{24} - iV\rho_{34} - i\frac{\Omega_{54}}{2}\rho_{54} + i\frac{\Omega_{24}}{2}\rho_{42} + iV\rho_{43} + i\frac{\Omega_{54}}{2}\rho_{45} - (W_4 + w_t)\rho_{44} \tag{4.54s}$$

$$\dot{\rho}_{45} = -i\frac{\Omega_{24}}{2}\rho_{25} - iV\rho_{35} - i\frac{\Omega_{54}}{2}\rho_{55} + i\frac{\Omega_{53}}{2}\rho_{43} + i\frac{\Omega_{54}}{2}\rho_{44} - (w_t - i\delta_3)\rho_{45} - \gamma_{45}\rho_{45} \tag{4.54t}$$

$$\dot{\rho}_{51} = \dot{\rho}_{15}^{*} \tag{4.54u}$$

$$\dot{\rho}_{52} = \dot{\rho}_{25}^{*} \tag{4.54v}$$

$$\dot{\rho}_{53} = \dot{\rho}_{35}^{*} \tag{4.54w}$$

$$\dot{\rho}_{54} = \dot{\rho}_{45}^{*} \tag{4.54x}$$

$$\dot{\rho}_{55} = -i\frac{\Omega_{53}}{2}\rho_{35} - i\frac{\Omega_{54}}{2}\rho_{45} + i\frac{\Omega_{53}}{2}\rho_{53} + i\frac{\Omega_{54}}{2}\rho_{54} - (W_5 + w_t)\rho_{55} + W_{45}\rho_{44} + W_{35}\rho_{33} \tag{4.54y}$$

Since continuous wave lasers were used in our experiment, the above equations can be solved under steady state conditions ($\dot{\rho}_I = 0$), simplifying them into a set of homogeneous linear equations. All of the equations of motion (4.54) can then be used to construct a matrix of the form

$$\dot{\mathrm{P}} = iL\mathrm{P} + iI \tag{4.55}$$

where L is a 25x25 matrix in which all experimental parameters are included, such as laser detunings, spin-orbit interactions, decay terms, and Rabi frequencies. P is a column vector containing 25 elements corresponding to the populations and coherences (P(1)= ρ_{11} , P(2)= ρ_{12} , P(3)= ρ_{13} ,… P(25)= ρ_{55}). The column vector I contains all inhomogeneous terms. As mentioned above, we can then set $\dot{\mathrm{P}}$=0, allowing the system

to be numerically solved for *P* using the process of matrix inversion. An exact solution can then be found for all populations and coherences.

4.6 Rabi Frequency M_J-dependence and Averaging Effects

Since states with the same *J* but different M_J have the same energy in the absence of an electric field, there are 2*J*+1 degenerate magnetic sublevels for each molecular state of rotational number *J*. The application of an external field lifts this degeneracy, and each magnetic sublevel experiences a slightly different transition dipole moment depending upon the molecules orientation to the laser field [12, 13]. Thus, for each sub-level M_J, a separate AT pair arises upon application of the coupling field to the system. The energy shift of each sublevel is $|M_J|$-dependent for the linearly polarized coupling field [12] and also depends upon the variety of the electronic transition. The rotational orientation factors, $F_{\Lambda\to\Lambda'}(J',M_J';J,M_J)$, of the transition dipole moment are included in the transition dipole moment expression in the form

$$\left\langle \mathrm{n}', \mathrm{v}', \mathrm{J}', \mathrm{M}_\mathrm{J}' \left| \mu \right| \mathrm{n}, \mathrm{v}, \mathrm{J}, \mathrm{M}_\mathrm{J} \right\rangle = \mu^{el} \left\langle \mathrm{v}' \middle| \mathrm{v} \right\rangle F_{\Lambda\to\Lambda'}(J',M_J';J,M_J) \tag{4.56}$$

where μ^{el} is the electronic part of the transition dipole moment, and $\left\langle \mathrm{v}' \middle| \mathrm{v} \right\rangle$ is the vibrational overlap or square root of the Franck-Condon factor. For our excitation scheme, the rotational factors for the Q branch of a $^1\Sigma \to {}^1\Pi$ transition and a P branch for a $^1\Sigma \to {}^1\Sigma$ transition, respectively, are

$$F^0_{\Sigma\to\Pi}(J' = J, M_J; J, M_J) = \frac{M}{\sqrt{J(J+1)}} \tag{4.57}$$

$$F^0_{\Sigma\to\Sigma}(J' = J-1, M_J; J, M_J) = \sqrt{\frac{J^2 - M_J^2}{(2J+1)(2J-1)}}\,. \tag{4.58}$$

The appropriate term for the M_J-dependent transition dipole moment is substituted into each Rabi frequency expression. Since the solution to the density matrix equations are M_J-dependent, a sum over the magnetic sublevels must be included in our simulation, which is of the form

$$\rho_{ii} = \sum_{M_J} \rho_{ii}^{(M_J)} \tag{4.59}$$

The frequency separation between the different M_J-dependent peaks may be resolved when the rotational number is very low [14]. For our case J=21, so with the available Rabi frequencies, the many sets of peaks simply result in a broadening in the typical observed Autler-Townes lineshape.

To account for the different thermal velocities of the molecules, an integration over the velocity distribution must also be performed, leading to the integration

$$\left\langle \rho_{ij} \right\rangle_{v_z, M_J} = \sum_{M_J} \int_{-\infty}^{\infty} \rho_{ij}^{M_J} (\mathrm{v}_z)\, N(\mathrm{v}_z)\, d\mathrm{v}_z \tag{4.60}$$

where $N(\mathrm{v}_z)$ is the one dimensional Maxwell distribution

$$N(\mathrm{v}_z) = \frac{1}{u_{mp}\sqrt{\pi}} e^{-\frac{v_z^2}{u_{mp}^2}}. \tag{4.61}$$

Here , u_{mp} is the most probable speed of the molecules of mass m at temperature T

$$u_{mp} = \sqrt{\frac{2kT}{m}}. \tag{4.62}$$

Since the laser electric field has a Gaussian spatial profile, a final averaging over the radial distribution of the field

$$E(r) = E_0 e^{-\frac{r^2}{w^2}} \tag{4.63}$$

can also be included. However, since the coupling field spot size was kept much larger than the spot sizes of the pump and probe lasers, the molecules in the interaction region experience a near uniform field, and this averaging was not included in our simulation. Calculations were further simplified since the hyperfine structure of the $1^3\Sigma_g^-$ state is negligible due to the electron density at the nuclei being zero [15, 16].

After completing all density matrix calculations and performing all averages, the fluorescence signal in our experiment can be simulated by plotting ρ_{33} and ρ_{44} (which correspond to the triplet and singlet detection channels, respectively) as a function of the detuning Δ_P from the perturbed $G^1\Pi_g(12,21f)$ state of the probe laser L2.

4.7 Conclusion

A density matrix formalism was developed which can be used to simulate the experimental data presented in this work. The density matrix approach was used to solve the various equations of motion for a five-level system interacting with three laser fields using the rotating wave approximation. Relaxation terms were included in the system of equations to account for all phenomenological decay terms such as spontaneous emission and the transit time of the molecules. Once all elements were obtained, a matrix was constructed from which solutions could be obtained under steady state conditions using matrix inversion. The exact solutions can then be used to plot populations and coherences of the system as a function of laser detuning, allowing for the comparison of experimental data with theoretical simulations.

References:

[1] M. O. Scully and M. S. Zubairy, *Quantum Optics*, (Cambridge University Press, Cambridge, 2002)

[2] E. Merzbacher, *Quantum Mechanics*, 3rd edition, (John Wiley and Sons Inc., Hoboken NJ USA, 1998)

[3] S. Stenholm, *Foundations of laser spectroscopy*, (Wiley-Interscience, New York, 1984)

[4] P. Meystre and M. Sargent, *Elements of Qauntum Optics*, 3rd ed., (Springer-Verlag, Berlin, 1999)

[5] A. Lazoudis, Ph.D. Thesis, Temple University (2005)

[6] C. J. Borde, andJ. L. Hall, *Laser Spectroscopy*, edited by A. Mooradian and R. G. Brewer (Plenum, New York, 1974)

[7] J. Sagle, R. K. Namiotka, J. Huennekens, J. Phys. B **29**, 2629 (1996)

[8] M. J. O'Calligan and A. Gallagher, Phys. Rev. A. **39**, 6190 (1989)

[9] M. J. O'Calligan and J. Cooper, Phys. Rev. A. **39**, 6206 (1989)

[10] L. Allen, and J. H. Eberly, *Optical Resonance and Two Level Atoms*, (Dover, New York, 1987)

[11] Teodora Kirova, Private Communication (2009)

[12] F. C. Spano, J. Chem. Phys. **114**, 276 (2001)

[13] R. N. Zare, *Angular Momentum: Understanding Spatial Aspects in Chemistry and Physics* (Wiley, New York, 1988)

[14] J. Qi, G. Lazarov, X. Wang, L. Li, L. M. Narducci, A. M. Lyyra, F. C. Spano, Phys. Rev. Lett. **83**, 288 (1999)

[15] Li, L., A. Yiannopoulou, K. Urbanski, A. M Lyyra, B. Ji, and W. C. Stwalley, T. An, J. Chem. Phys. **105**, 6192 (1996)

[16] A. Yiannopoulou, B. Ji, L. Li, M. Li, K. Urbanski, A. M. Lyyra, W. C. Stwalley, G.-H. Jeung, J. Chem. Phys. **101**, 3581 (1994)

CHAPTER 5

EXPERIMENTAL DETAILS AND RESULTS

5.1 Introduction

As previously discussed, the goal of much recent research in modern quantum mechanics has been toward achieving coherent quantum control. This work involves the quantum control of a pair of singlet and triplet states in Li_2 which are initially weakly mixed by the spin orbit interaction. Experimental results reveal that one can control the amount of mixing between two perturbed states by varying the strength of an applied coupling field which is resonant with the singlet component of the perturbed state. A description of the experimental equipment and parameters used to obtain the experimental data are presented in this chapter. The effect that the coupling field has upon the population of the mixed levels at various powers will be shown. The mixing coefficients are calculated for the cases of no coupling field and when the coupling field was 750mW.

5.2 Diatomic Lithium Potential Curves

The potential energy curves of Li_2 for the states used in this experiment are displayed in Figure 5.1. As illustrated by the figure, the $A^1\Sigma_u^+$ and $b^3\Pi_u$ states have the same dissociation limit (2s + 2p), as do the $G^1\Pi_g$, and $1^3\Sigma_g^-$ states (2p + 2p). The illustrated crossings of potential curves results in the mixing of rovibrational levels from

the $A^1\Sigma_u^+$ and $b^3\Pi_u$ states, and from the $G^1\Pi_u$ and $1^3\Sigma_u$ states, by the spin orbit interaction. As discussed in section 3.5, this mixing occurs between two closely spaced levels having the same rotational number. A mixed $A^1\Sigma_u^+ \sim b^3\Pi_u$ pair was used in previous work [1], while in this work a perturbed pair between the $G^1\Pi_u \sim 1^3\Sigma_u^-$ states was chosen. A list of perturbed levels that have been found in molecular lithium can be found in Refs. [2-4].

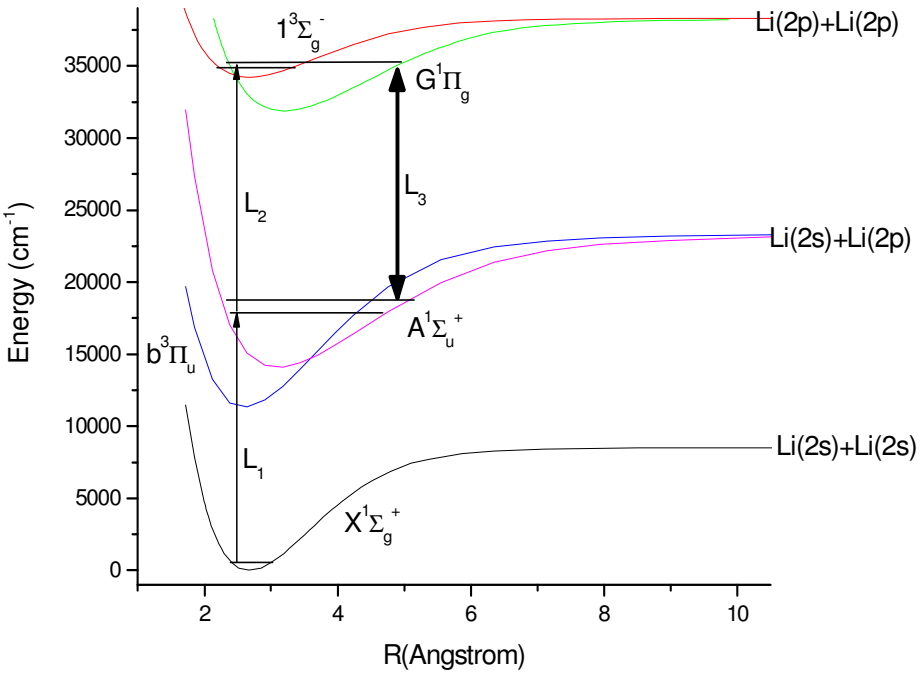

Figure 5.1 Potential energy curves of $^7Li_2$ as a function of internuclear distance *R*. The data from which the $X^1\Sigma_g^+$, $A^1\Sigma_u^+$, $b^3\Pi_u$, $G^1\Pi_g$, and $1^3\Sigma_g^-$ curves were constructed can be found in references [5-10].

5.3 Experimental Details

Lithium gas was produced in a five-arm, stainless steel heatpipe oven. Three heaters were positioned on the sidearms and the bottom reservoir at the center of the heatpipe and wrapped in insulation. The side arm heaters were 280hm heaters from Lindberg, and the center heater was an ARI heater (BXX-093B38-4T). The voltage applied to the center and side heaters was 95V and 85V, respectively. Most of the vapor produced in the heatpipe is atomic lithium, with about 5% of the atoms forming molecular lithium. A small reservoir is located at the bottom center of the heatpipe to allow the lithium to pool in the region where the laser beams are focused and from which light is detected. Steel mesh was placed inside each horizontal arm to allow the liquid lithium to circulate smoothly inside the heatpipe. The end of each arm of the heatpipe was covered with an o-ring vacuum seal in the flange holding the window in place. The arms of the heatpipe were water-cooled to prevent the lithium from condensing on the windows. Argon gas was added as a buffer gas. The lithium vapor pressure varied from 100-200 mTorr, and the temperature was ~850K.

The temperature was calculated from the Doppler profile obtained while scanning the pump laser over the pump laser transition. Using equation 5.1, which is based on the Maxwell-Boltzmann distribution, we were able to determine the temperature of our system

$$T = \left(\frac{\Delta\omega c}{2\omega_0}\right)^2 \frac{m}{2k \ln 2} \tag{5.1}$$

where $\Delta\omega$ is the full width at half maximum (FWHM), c is the speed of light, ω_0 is the center frequency, m is the molecular weight of the lithium dimer in kilograms, and k is

Boltzmann's constant. The calculated temperature for the heater voltage settings of 85V/95V/85V (side/center/side, respectively) was 856K. The singlet fluorescence detection channel used was 672.06 nm, which corresponds to the $A^1\Sigma_u^+$ (11, 21) → $X^1\Sigma_g^+$(5, 20) transition. The Doppler profile obtained while scanning the pump laser can be seen in Figure 5.2. To ensure an accurate temperature calculation, the pump laser was scanned at very low power (~1mW) to mitigate any power broadening effects, and the scan was taken very slowly to minimize background noise. The Vernier etalon (VET) signal from the laser wavemeter was also collected throughout every scan in this experiment to ensure that the scan was smooth and that no mode hops occurred.

5.4 Experimental Setup

The experimental setup is shown in Figure 5.3. The pump (L1), probe (L2), and coupling (L3) lasers were all Coherent Autoscan 699-29 ring dye lasers. The bandwidth of each laser is 0.5MHz. All three lasers were pumped by separate pump lasers manufactured by the Coherent Laser Group operated at about 6W output power. The pump laser L1was pumped by a Sabre DBW-25 argon ion laser, while the probe and coupling lasers were pumped with Coherent Verdi V10 lasers. All lasers were linearly polarized in the same direction. The pump laser was operated with dicyanomethylene (DCM) dye, and the probe and coupling lasers were operated with Rhodamine 590 (R6G) dye. The pump and coupling lasers co-propagated, while the probe laser counter-propagated. For phase-sensitive detection, a mechanical chopper was used to modulate the pump laser beam with a frequency ~1000Hz. Neutral density filters were placed in the paths of each beam to allow the desired power of each laser to enter the heatpipe.

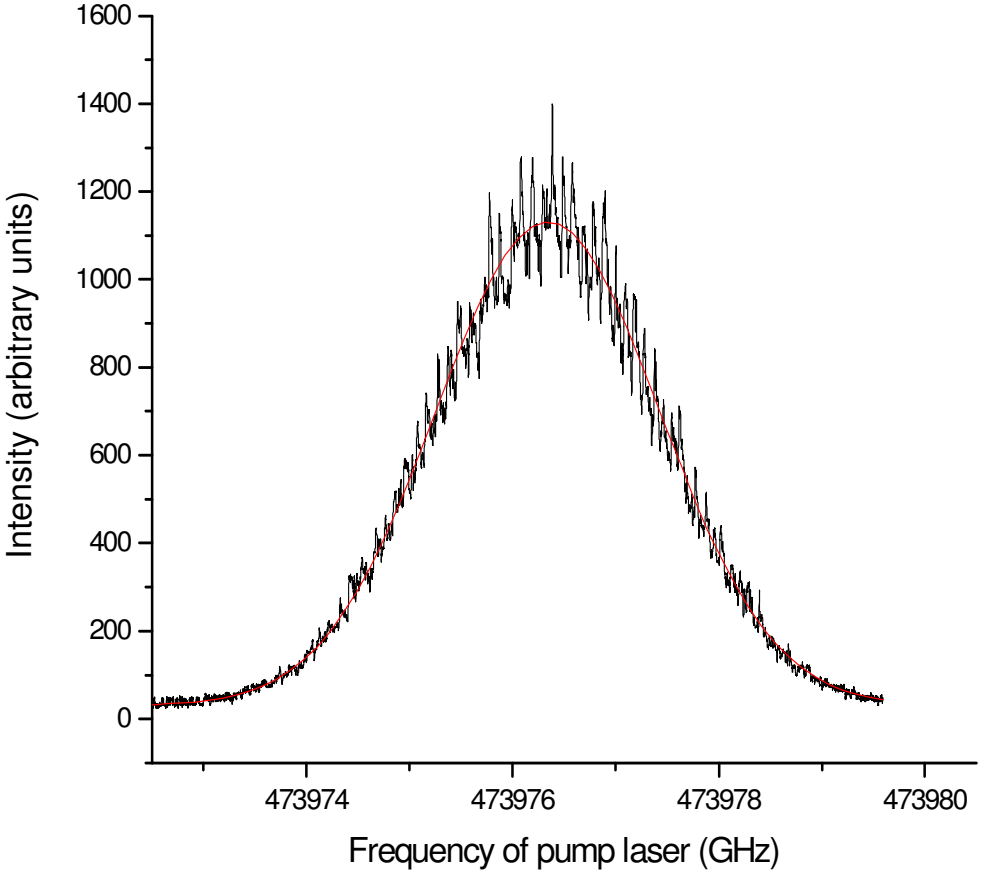

Figure 5.2 The Doppler broadened profile obtained while scanning the pump laser. The power of the pump laser was very low (~1mW) in order to minimize any power broadening effects. The singlet fluorescence detection channel used corresponded to a wavelength of 672.06nm. Using equation (5.1), the temperature calculated from this Doppler profile was 856K.

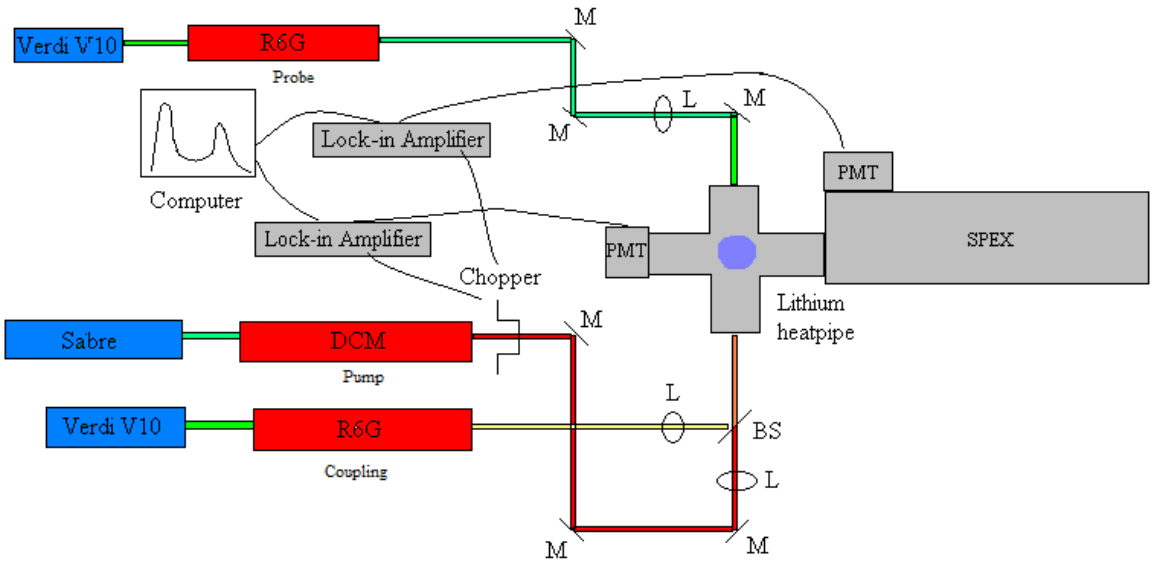

Figure 5.3 Experimental setup for the S-T mixing experiment. The pump and coupling lasers co-propagated, while the probe beam counter-propagated. The OODR fluorescence was detected in two different ways. The total triplet fluorescence was detected by the side PMT using blue filters, and the singlet channel fluorescence was detected using a SPEX monochromator, which allows for the detection of a single rovibrational singlet transition.

Two fluorescence detection channels were used during our experiment: the total triplet fluorescence, which arose from the triplet character of the singlet-triplet mixed pair, and a single-channel singlet fluorescence signal, which originated from the singlet character of the singlet-triplet mixed pair. Since most of the population in our experiment resided in the singlet state, collecting the total triplet fluorescence allowed for a strong triplet channel signal. The total triplet channel fluorescence was collected by a photomultiplier tube (R928) mounted on the top arm of the heatpipe. The high voltage

supplied to the PMT was 500V. Two blue filters (Kopp Glass Inc. 5433 and 5543) were placed in front of the PMT to prevent the red and yellow scattered laser photons from reaching the detector, allowing for the detection of only the violet side fluorescence signal. The $1^3\Sigma^-_g$ state can only fluoresce to the vibrational levels of the $b^3\Pi_u$ state, thus the total range of wavelengths for the triplet fluorescence is 440-595nm, with the blue filters mostly blocking the transmission of wavelengths above ~550nm. The singlet channel fluorescence signal was collected while monitoring a single rovibrational singlet transition (i.e. one wavelength). The singlet channel fluorescence was detected using a Spex 1404 double grating monochromator, a cooled photomultiplier tube (PMT), and lock-in amplifier (SR 850) system. After the fluorescence from the center of the heatpipe entered the entrance slit of the Spex, the photons went through a series of gratings and slits, allowing only the desired wavelength photon to reach the cooled PMT. The voltage applied to the PMT was 1000V. The signal from this PMT was collected by a lock-in amplifier, which sent the signal to the computer which controls the scanning laser. The computer then displayed a graph of fluorescence intensity vs. frequency of the scanning laser.

All three laser beams were focused and overlapped at the center of the heatpipe oven. Optimal overlap was achieved by first maximizing the OODR signal from the pump and probe beams, and then carefully overlapping the coupling field so that, at relatively low power (~200mW), the AT splitting was maximized. The coupling field must be at low power for this step, since at high powers the AT splitting becomes so large

and broadened that slight changes in the position of the coupling field result in minimal differences in the shape of the splitting (see Sec.3.2). The powers for all lasers were measured with a Coherent Lasermate D power meter, which has an accuracy of ±1% of the reading. The spot sizes of the pump, probe and coupling fields at the center of the heatpipe were 250 μm, 300 μm, and 425 μm, respectively. Exact spot sizes were achieved using either one lens or two lenses in combination and measured using the razor blade method [11]. The spot size or beam waist *w(z)* is defined as the radial distance between the points on the Gaussian profile where the intensity is $1/e^2$ of its largest value, I_0 (see Figure 5.4). The intensity of the laser beam is given by

$$I(r,z) = I_0(z)e^{\frac{-r^2}{w^2(z)}} \tag{5.2}$$

from which the spot size *w* is found to be

$$w = \frac{1}{\sqrt{2C}}(d_{75} - d_{25}) \tag{5.3}$$

where *C* is the solution to $erf(C) = \frac{1}{2}$, which is found to be $C \approx 0.47$, and d_{75} (d_{25}) is the position of the razor blade when the transmitted power is 75% (25%) of the maximum laser power. Thus, the spot sizes were found by slowly sweeping a razor blade, which was mounted on a translational stage attached to a micrometer dial, across the laser beam profile and recording $d_{75} - d_{25}$ for each beam at a location equal to the distance to the center of the heatpipe. The spot sizes were measured both vertically and horizontally to ensure a symmetric profile. The error of all spot size measurements is 10 μm. The spot sizes were chosen so that the electric field of the coupling laser would be uniform in the

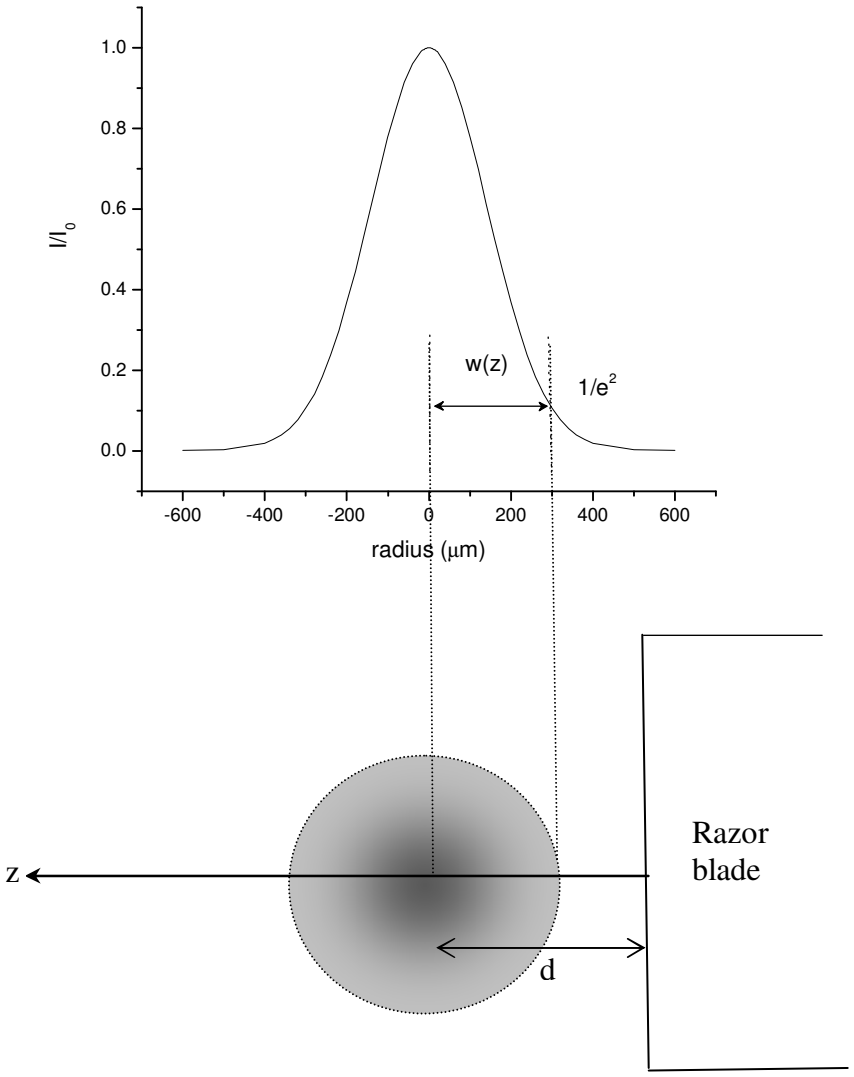

Figure 5.4 Laser beam spot size *w* is defined as the radial distance between the points on the Gaussian profile where the intensity is $1/e^2$ of its largest value, I_0. The razor blade mounted on a translational stage equipped with a micrometer dial is slowly swept across the beam profile to determine the spotsize using equation (5.3).

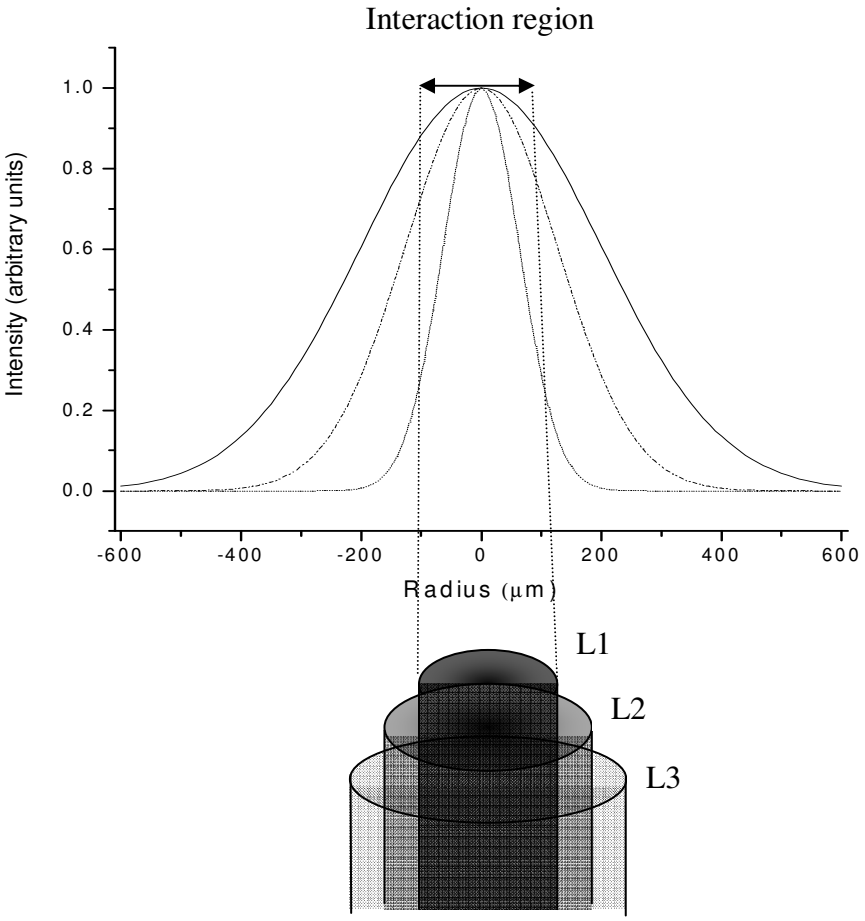

Figure 5.5 Laser beam profiles of the pump (L1), probe (L2), and coupling (L3) lasers. Spot sizes of the three laser beams were chosen to ensure that the coupling laser's electric field (and therefore Rabi frequency) was uniform over the interaction region.

region where the pump and probe beams interact. This can be seen graphically in Figure 5.5. A uniform electric field of the coupling laser throughout the interaction region provides for a constant Rabi frequency.

5.5 Doppler Broadening Considerations

Previous work related to S-T mixing control [1] used a five-level extended lambda system where the mixed pair involved the intermediate levels (Figure 5.6). Even though the pump laser is set to one specific frequency, this energy scheme included Doppler broadening effects, since both the singlet and triplet mixed levels are under the Doppler width of ~ 2.4GHz (see Figure 5.7). The pump laser was set on resonance with the singlet component, therefore only the molecules travelling perpendicular to the beam (with velocity component $v_z = 0$) participate in the singlet absorption. The same laser frequency is also absorbed by the molecules which have a significant velocity component in the same direction as the laser beam for the triplet component absorption, since they are red shifted from the resonance of the triplet transition for the laser tuned to resonance on the singlet. Having two active velocity groups (which becomes three active velocity groups when the singlet is AT split by the coupling field) could complicate the results of the singlet-triplet mixing effect under investigation.

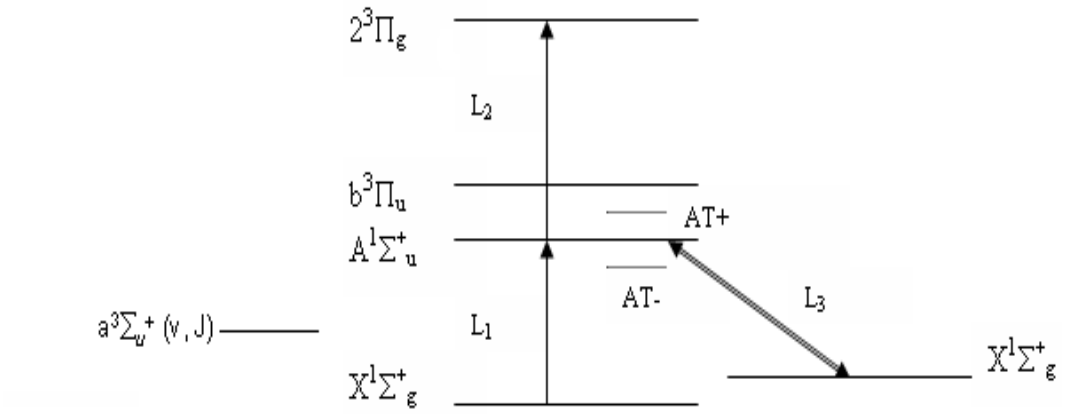

Figure 5.6 Energy scheme for previous work [1]. The singlet-triplet mixed levels are the two intermediate levels ($A^1\Sigma_u^+$ and $b^3\Pi_u$) in the system. The energy separation between the $A^1\Sigma_u^+$ and $b^3\Pi_u$ levels is 680MHz (exaggerated for clarity in the diagram), well within the typical Doppler broadened linewidth for Li_2 of 2.4GHz.

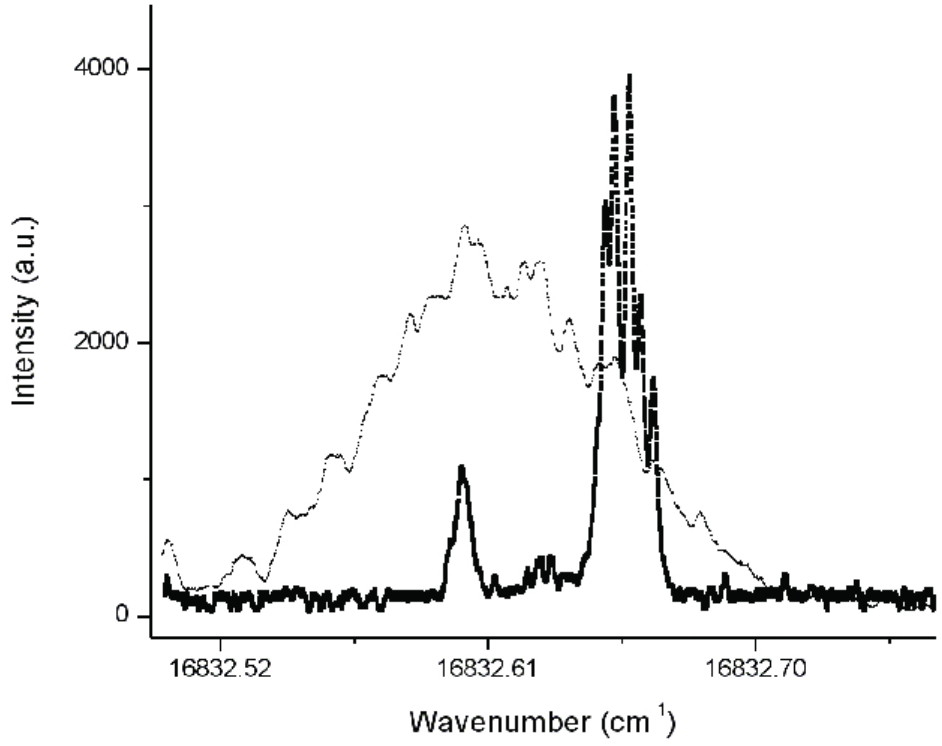

Figure 5.7 Doppler broadening effects from Ref. [1]. The thin line shows the Doppler broadened profile collected as the pump laser was scanned over the $A^1\Sigma_u^+(17,15)$~$b^3\Pi_u(22,15)$ – $X^1\Sigma_g^+(3,14)$ transition. The bold line shows the OODR signal when the copropagating probe laser was held at the $2^3\Pi_g$ (19,15)- $A^1\Sigma_u^+(17,15)$ resonance, and the pump laser was scanned around the $A^1\Sigma_u^+$~ $b^3\Pi_u$ - $X^1\Sigma_g^+$ transition. The singlet state is on the left, and the triplet state is on the right (note the hyperfine structure). Since the singlet and triplet states are both under the Doppler profile, even when the pump laser was set to the singlet state transition, both the singlet and triplet states are simultaneously populated from the ground state. This fact results in the intermediate mixed states being populated by two velocity groups.

5.6 Excitation Scheme

To eliminate the Doppler broadening effects discussed in Sec. 5.5, an extended lambda system (Figure 5.8) was chosen, in which our mixed singlet-triplet perturbed pair were the highest energy levels. The pump laser, L1, excited the lithium molecules from the thermally populated ground state to the intermediate state in the transition $A^1\Sigma_u^+$ (11, 21) $\leftarrow X^1\Sigma_g^+$(2, 22). When the pump laser is set to the center of this transition, only $v_z = 0$ molecules are excited. The transition frequency was experimentally measured to be 15,810.158 cm^{-1}. The probe laser, L2, was scanned and excited molecules from the $A^1\Sigma_u^+$ (11, 21) level to the $1^3\Sigma_g^-$ (1,21f) and $G^1\Pi_g$ (12, 21) levels. The transition energy between $A^1\Sigma_u^+$ (11, 21) and $1^3\Sigma_g^-$ (1,21f) was 17,666.136 cm^{-1}, while the transition energy between $A^1\Sigma_u^+$ (11, 21) and $G^1\Pi_g$ (12, 21) was 17,666.162 cm^{-1}. The coupling field frequency was held fixed to 17,026.872 cm^{-1}, corresponding to the transition $G^1\Pi_g$ (12, 21) $\leftarrow A^1\Sigma_u^+$ (14, 21). Approximate transition frequencies were calculated using the quantum program LEVEL 8.0 [12], which solves numerically the radial Schrödinger equation. All experimental laser frequencies were calibrated against the molecular Iodine Atlas [13, 14], with an uncertainty of 0.005 cm^{-1}. All vibrational and rotational quantum numbers were confirmed by performing a resolved fluorescence scan while the laser was set on each transition. Note that the energy separation between the two mixed levels is only 780MHz. The coupling field Rabi frequency obtained in our case was about 500MHz. Such comparable values of energy separation and Rabi frequency allowed significant control effects to be seen in our experiment.

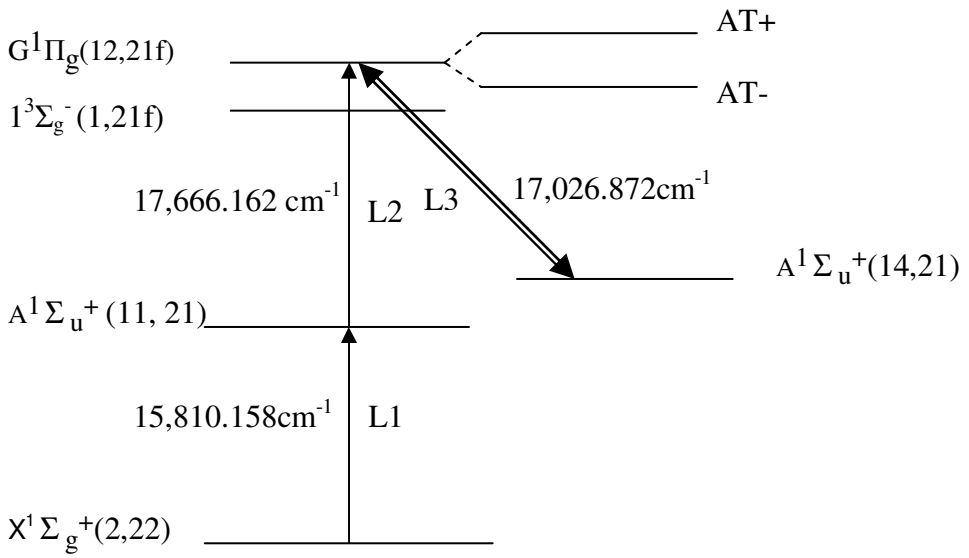

Figure 5.8 Excitation scheme for the S-T mixing experiment. The upper singlet $G^1\Pi_g$ (12,21f) and triplet $1^3\Sigma_g^-$ (1,21f) mixed states are separated by 720MHz. The width of the energy separation of this mixed pair is exaggerated in the diagram for clarity.

The power of the pump laser varied from 50 μW to 10mW, while the probe laser power varied from 1mW to 25mW. The power was kept low to avoid any power broadening effects. Different sets of pump and probe powers were tested to see which combination yielded the cleanest signal. Since the AT splitting is proportional to the Rabi frequency of the laser (i.e. the electric field amplitude and transition dipole moment matrix element, μ, between the two levels involved), the coupling field transition was chosen to have its frequency near the center of the tuning curve of the dye. LEVEL 8.0 was used to calculate the transition dipole moments between all $G^1\Pi_u$ (12, 21) →

A (v, 21) levels within the dye range. The frequency difference between the two levels with the largest μ was chosen.

To observe the degree to which the coupling field affected the mixing coefficients in our system, two fluorescence channels were detected during our experiment: single channel fluorescence, which arises from the singlet character of the $G^1\Pi_u$ (12, 21f) ~ $1^3\Sigma_g^-$ (1,21f) mixed levels, and total triplet fluorescence, which arises from the triplet character of the $G^1\Pi_u$ (12, 21f) ~ $1^3\Sigma_g^-$ (1,21f) mixed levels. The singlet detection channel was 559.4 nm, which corresponds to the $G^1\Pi_u$ (12, 21f) → A(10,21) transition. The triplet fluorescence from the mixed levels is to the $b^3\Pi_u$ state potential well, since the $1^3\Sigma_g^-$ state cannot radiatively decay to the $a^3\Sigma_u^+$ state [9]. Both channels were collected simultaneously during each scan and used to determine the mixing coefficients. Since the singlet channel fluorescence from both the singlet and triplet mixed levels arises from pure singlet transitions, the singlet channel is more reliable for intensity calculations. As the coupling field splits the $G^1\Pi_u$ (12, 21f) level, one of the AT components is pushed closer toward the triplet state. This causes the nominally triplet state to become more singlet in character, and therefore more singlet character fluorescence is detected from the nominal triplet state. The triplet character fluorescence, on the other hand, is not as straightforward, since other effects must be considered. Pushing one of the singlet AT components toward the triplet state has two simultaneous effects: (1) the singlet character of the nominally triplet state increases (therefore the triplet fluorescence would be expected to *decrease*) (2) the population being pumped into the upper nominal triplet state from the intermediate singlet state increases (from which we would expect the

triplet fluorescence to i*ncrease,* since the overall population of the nominal triplet state has increased). Since these effects are in opposition to one another, a consistent trend in the triplet character fluorescence from the nominally triplet state as the coupling field power increased was not observed. This inconsistency may have also resulted from daily variableness in vapor pressure (130–250 mTorr), fluctuations in pump and probe powers due to laser instability, variable laser frequencies (100MHz frequency drift per hour), collisions, and/or other dephasing factors [15]. As a result, the uncertainty in the triplet channel intensity calculations is substantial. The triplet channel fluorescence from the nominally singlet state, however, does clearly display the singlet and triplet character associated with each component of the Aulter-Townes split pair.

5.7 Experimental Data

For each scan, the pump laser was held at the $A^1\Sigma_u^+$ (11, 21) ←$X^1\Sigma_g^+$(2, 22) resonance, while the probe laser was scanned across the $G^1\Pi_u$ (12, 21f) ← $A^1\Sigma_u^+$ (11, 21) transition. The stepsize for the scanning laser was 2MHz, with the total scan width being 2.5 GHz. The signal for each step was sampled 500 times, and each scan was typically five minutes in duration. When the coupling field was absent from the system, the peaks resulting from the $1^3\Sigma_g^-$ (1,21f) ←$A^1\Sigma_u^+$ (11, 21) and $G^1\Pi_g$ (12, 21f) ←$A^1\Sigma_u^+$ (11, 21) transitions were seen in a typical OODR spectrum. When the coupling field was applied to the system at the $G^1\Pi_u$ (12, 21f) ← $A^1\Sigma_u^+$ (14, 21) transition, the $G^1\Pi_u$ (12, 21f) level split into an Autler-Townes pair. As the left component of the AT pair (see Fig 5.9) was pushed toward the nominally triplet state, the triplet state gained more singlet character, increasing the singlet character fluorescence from the triplet state. The black trace in

Figure 5.9 indicates the *singlet* character population of the nominally triplet and nominally singlet levels when the coupling field is *absent*. The red trace displays the *triplet* character population of the nominally triplet and nominally singlet levels when the coupling field is *absent*. The blue line denotes the *triplet* character of the nominally triplet and nominally singlet states populations when a strong coupling field is *applied* to the system. The green line denotes the *singlet* character of the nominally triplet and nominally singlet state populations when the strong coupling field is *applied*. Note that even when the coupling field is exactly on resonance, the AT splitting has an asymmetric line shape. This asymmetry is displayed in both the singlet and the triplet detection channels, with the asymmetry being reflected in each detection case. When the singlet channel was detected, the right component of the AT split nominally singlet state was larger than the left component; when the triplet channel was detected, the left component of the AT split pair was larger than the right component. This indicates that the left AT component (the one nearest the triplet state) has more triplet character, and the right AT component has more singlet character.

The AT peaks also broaden as the coupling field power increases due to the M_J-dependence of the Rabi frequency [16]. The application of the coupling field to the system removes the degeneracy of the magnetic sublevels, and the individual M_J components compose the absorption spectrum. The lineshape is thus a superposition of the individual M_J components which experience varying degrees of AT splitting. Note also the leftward shift of the nominally triplet state peak when the coupling field is

applied. This shift is most likely due to the non resonant AC stark shift induced by the coupling field.

Figure 5.10 reveals the dependence of the population of singlet and triplet mixed levels on varying levels of coupling field power. All data in Figure 5.10 was collected through singlet channel fluorescence detection. The black line denotes populations of the nominal singlet and nominal triplet states when no coupling field was present. The colored lines signify the populations of each state at various levels of coupling field power. As the coupling field was increased, the nominal triplet state gains more singlet character; thus, the peak height/area increases due to more singlet population being pumped from the ground and intermediate states into the upper nominal triplet state. When the coupling field was held at relatively low power, the increase in singlet character of the nominal triplet state is very small. Once the coupling laser reached powers above 500mW, the population of the nominal triplet state increased more dramatically. The pump laser frequency moved slightly in between scans, causing the $1^3\Sigma_g^-$ (1,21f) $\leftarrow A^1\Sigma_u^+$ (11, 21) and $G^1\Pi_g$ (12, 21) $\leftarrow A^1\Sigma_u^+$ (11, 21) transitions to be in slightly different positions each time. Consequently, the leftward shift of the $1^3\Sigma_g^-$ (1,21f) state peak as the coupling field power increases is not apparent. The singlet channel fluorescence of the nominal triplet state did, however, consistently increase with coupling field power, and the asymmetry of the AT pair is also seen to grow as a function of coupling field power.

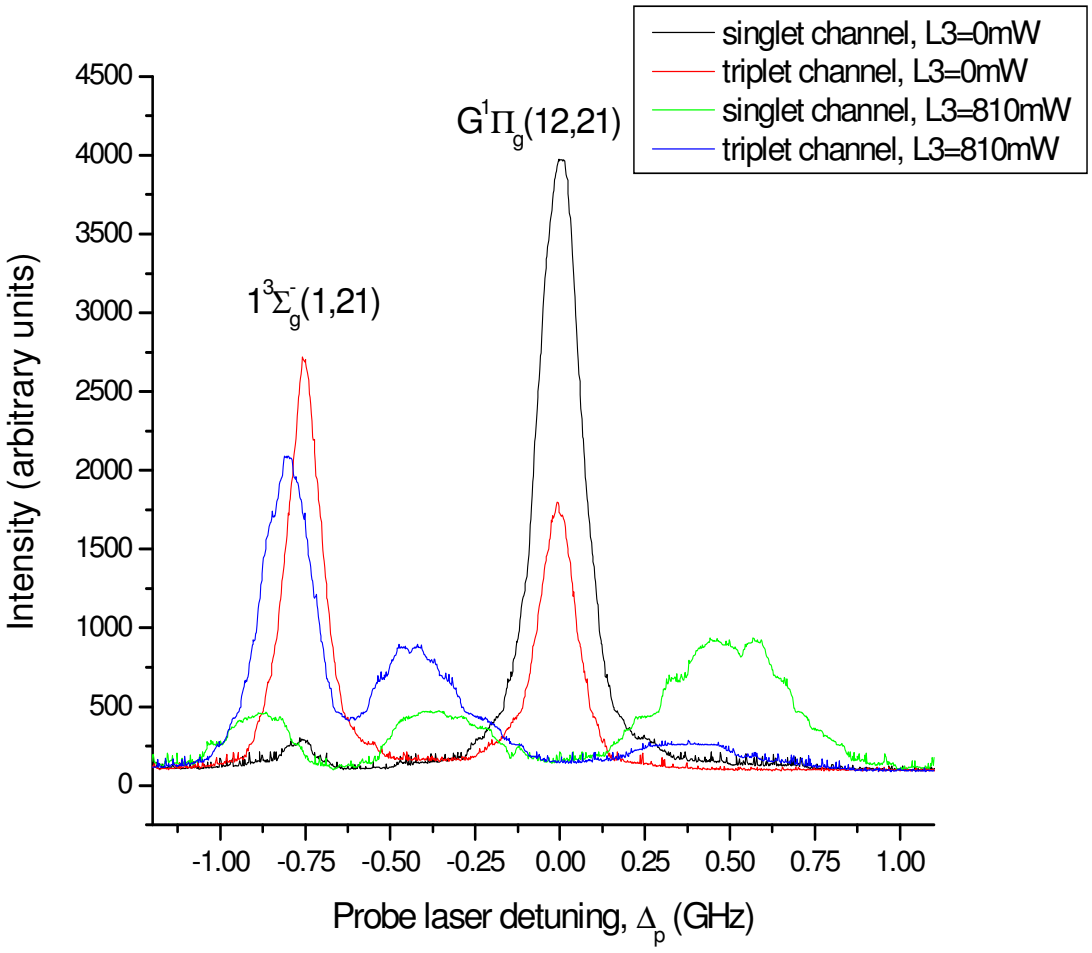

Fig 5.9. Experimental total fluorescence of the $1^3\Sigma^-_g$ (1, 21) and $G^1\Pi_g$ (12,21f) levels as a function of probe laser detuning from the $G^1\Pi_g$ (12,21f) - $A^1\Sigma_u^+$(11, 21) transition, monitored through triplet fluorescence and singlet fluorescence channels. When the strong coupling field is applied, the singlet state splits into two AT components. As the singlet-characterized left AT component is pushed toward the nominally triplet state, the triplet state gains more singlet character, indicated by the increases in singlet channel fluorescence from the $1^3\Sigma^-_g$ (1, 21) state. The asymmetry of the AT pair reflects the singlet and triplet character of each component. The coupling field power was 810mW outside (750mW inside) the heatpipe.

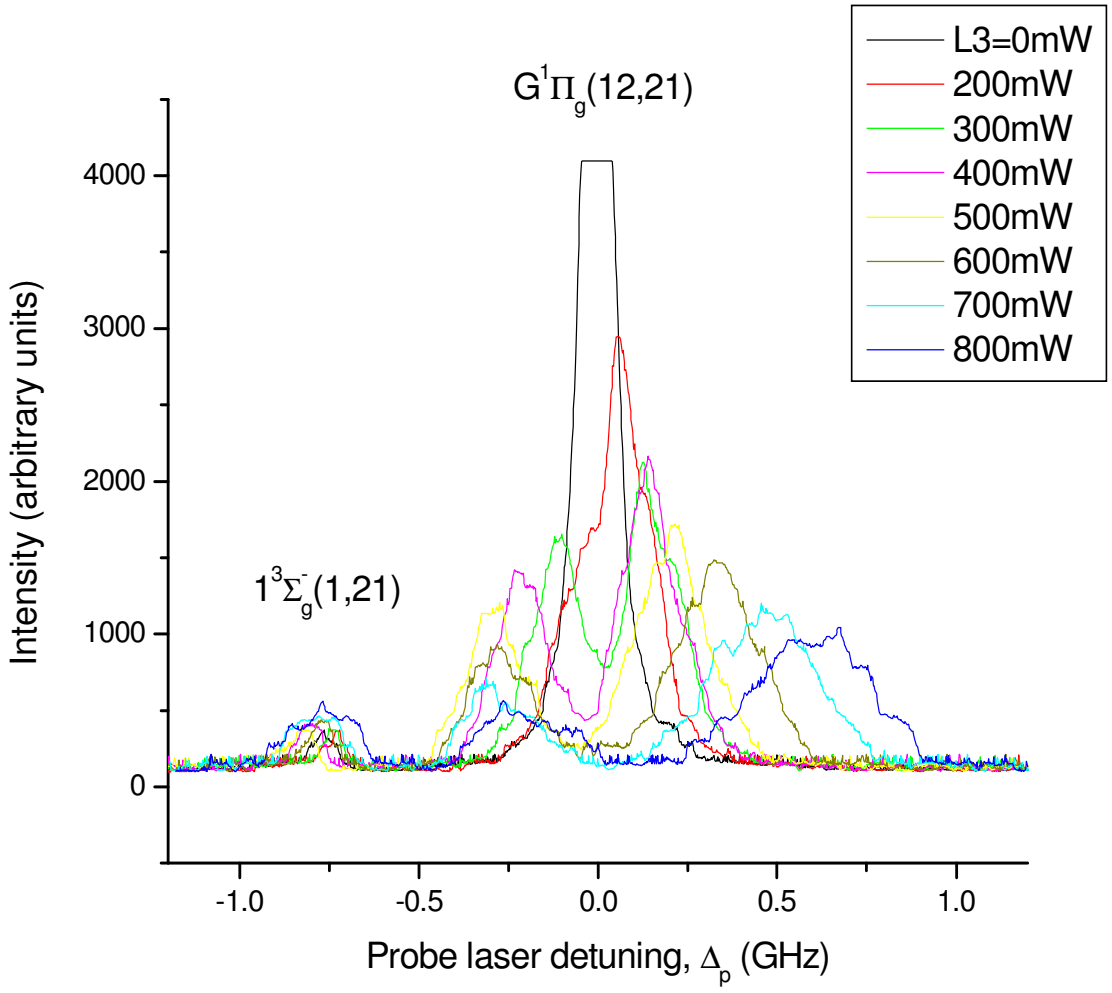

Fig 5.10. Experimental singlet channel fluorescence of the $1^3\Sigma^-_g(1, 21)$ and $G^1\Pi_g$ (12,21f) levels as a function of probe laser detuning from the $G^1\Pi_g(12,21f)$ - $A^1\Sigma_u^+(v=17, J=15)$ transition at varying coupling field powers. All coupling field powers were measured outside the heatpipe. As the coupling field power was increased, the singlet character fluorescence from the $1^3\Sigma^-_g(1, 21)$ state increased. At high coupling field powers, the effect becomes more pronounced. The asymmetry of the AT components also becomes more distinct as the coupling field power grows.

From these spectra we can clearly conclude that the singlet population of the nominally triplet state increases as coupling field power increases. This increase occurs because the strong coupling field splits the nominally singlet state into two AT components, pushing the singlet-characterized AT components closer toward the nominally triplet state. As the singlet character of the nominally triplet state is increased, the spin-orbit interaction between the mixed states is enhanced, allowing more population to be pumped from the singlet ground and intermediate states into the nominally triplet state.

5.8 Simulations

The experimental data may be simulated using the density matrix equations of motion (equations 4.54*a*-*y*) presented in Chapter 4, and simulations are currently in progress [17]. The parameters required for the simulation, including laser powers, spotsizes, Franck-Condon Factors, transition dipole moments, and Rabi frequencies can be found in Table 5.1. Since power is lost due to reflection when the laser beam enters the heatpipe window, a loss factor was determined by measuring the laser power directly before the entrance window and directly after the exit window. The loss due to both sides of one window reflection was found to be 7.42%, therefore the actual power in the interaction region was determined by the formula

$$P_{actual} = 0.926 P_{meas} .$$

The lifetimes for each rovibrational level used in the simulation were calculated by the formula

$$\tau = \frac{1}{\sum_{v',v''} A_{v',v''}}$$

where the sum is over all possible transitions from an initial state (v', J') to a final state (v'', J''), and $A_{v',v''}$ is the Einstein coefficient for the rate of spontaneous emission found by the expression

$$A_{v',v''} = 3.1361891\times10^{-7}\,\frac{S(J',J'')}{2J'+1}\nu^3\,|\langle\Psi_{v',J'}\,|\,M(R)\,|\,\Psi_{v'',J''}\rangle|^2.$$

Here $S(J', J'')$ are the Hönl-London rotational intensity factors, *v* is the emission frequency in cm^{-1}, and *M(R)* is the transition dipole moment in Debye. All Einstein *A* coefficients were calculated using Level 8.0. The $A^1\Sigma_u^+$ state can only spontaneously emit to the $X^1\Sigma_g^+$ state, and the $1^3\Sigma_g^-$ state only fluoresces to the $b^3\Pi_u$ state (other transitions contribute negligibly to the lifetime due to the ν^3 factor), making only one summation necessary for those respective lifetime calculations. The $G^1\Pi_g$ state can spontaneously emit to the $A^1\Sigma_u^+$ state as well as the $B^1\Pi_u$ state, therefore the total lifetime was found after two summations were determined. The lifetimes for the pure rovibrational levels used in our energy scheme were found to be as follows:

$A^1\Sigma_u^+$ (11,21) - 18.78ns

$A^1\Sigma_u^+$ (14,21) - 18.9ns

$G^1\Pi_g$ (12,21) - 16.21ns

$1^3\Sigma_g^-$ (12,21) - 9.27ns

Table 5.1 Parameters used in simulation program to model experimental data.

Laser	L1 (pump)	L2 (probe)	L3 (coupling)
Transition energy (cm^{-1})	15,810.158	17,666.136 ($1^3\Sigma_g^-$), 17,666.162 ($G^1\Pi_g$)	17,026.872
Power (mW)	0.088	6.02	750
FCF	0.0675	0.137	0.274
TDM (Debye)	-2.05	-1.80	3.31
Rabi frequency/2 (MHz)	8.81	53.33	702
Spot size (μm)	250	300	425

5.9 Mixing Coefficients

As described in Section 3.6, the mixing coefficients of a state indicate how much singlet character and how much triplet character the state has and can be determined using equation (3.30). To determine the magnitude of the change in the singlet-triplet mixing induced by the coupling field, the peak areas of the fluorescence from the nominally singlet and nominally triplet states were integrated when the coupling field was both absent and present for both singlet and triplet detection channels. Both components of the AT split peaks must be included when finding the intensity from the "singlet" state. Introduction of the strong coupling field into the heatpipe introduced more light scatter into the system, and therefore more background noise to the signal. In

order to accurately compare mixing coefficient values when the coupling field was both present and absent, the background was subtracted from the data so that the baseline was zero for each area measurement. Due to the overlapping of peaks and collisional effects to the triplet state, the uncertainties of the mixing coefficients are considerable.

When the coupling field was absent, the mixing coefficients were found to be

$$\alpha^2 = 0.87 \qquad \beta^2 = 0.13$$

meaning that the nominally singlet state is 87% singlet and 13% triplet, and the nominally triplet state is 87% triplet and 13% singlet. Adding a relatively weak coupling field did not induce a significant change in peak areas for either the singlet or the triplet, therefore mixing coefficients for smaller powers were not determined. The largest change in mixing coefficients occurred when the coupling field was at largest power (750mW), in which case the mixing coefficients were found to be

$$\alpha^2 = 0.73 \qquad \beta^2 = 0.27$$

Thus, the application of the coupling field to the system enhanced the singlet character of the nominally triplet state by 112%.

5.10 Future work

A possibility for future work in this area of singlet-triplet mixing control is to investigate the role that valence electron spin polarization plays in photochemical reactions [18]. For example, a photochemical reaction can occur when an excited lithium molecule reacts with a zinc atom to create a lithium atom and LiZn molecule in the reaction $Li_2^* + Zn \rightarrow LiZn^* + Li$.

Since the $G^1\Pi_g$ and $1^3\Sigma_g^-$ states used in this work are nearly resonant in energy with the $3^2\Sigma^+$ and $2^2\Pi_g$ states of the LiZn excimer, an experiment that uses the same energy scheme to create excited state lithium molecules required for the reaction has been proposed [18]. The energy diagrams for both molecules are presented in Figure 5.11. The dissociation limits for the ground states of Li(2s)+Li(2s) and Li(2s)+Zn($3d^{10}4s^2$) are the same. The goal of the experiment would be to investigate the effect that controlled spin change of Li_2^* has on the reactivity of the molecules excited to such a pair of mixed levels. A pump and probe laser will be used to create the excited state lithium molecules in a heatpipe containing both lithium and zinc. The photochemical reaction would then produce LiZn, which emits fluorescence in the wavelength range of around 400nm, corresponding to the bound-bound and bound-free transitions LiZn $3^2\Sigma^+ \rightarrow X\ ^2\Sigma^+$ or $2^2\Pi_g \rightarrow X\ ^2\Sigma^+$. By monitoring this bound-bound and bound free fluorescence for different spin cases of the reactant, one can determine how much LiZn was produced [19]. The initial test cases would involve having the reactant lithium in the pure singlet and pure triplet states.: $Li_2(\uparrow\downarrow) + Zn \rightarrow LiZn + Li$ and $Li_2(\uparrow\uparrow) + Zn \rightarrow LiZn + Li$.

If the fluorescence signal from the LiZn indicates that a different amount of product formed for each of the cases, the next step would be to monitor the LIF when the excited lithium has partial singlet and triplet character. This would be achieved by altering the strength of the coupling laser applied to the singlet-triplet mixed levels. Thus, the effect of the coupling laser L_3 on the singlet and triplet character of the mixed pair of levels of Li_2^* at the entrance channel to the transition state could be tested.

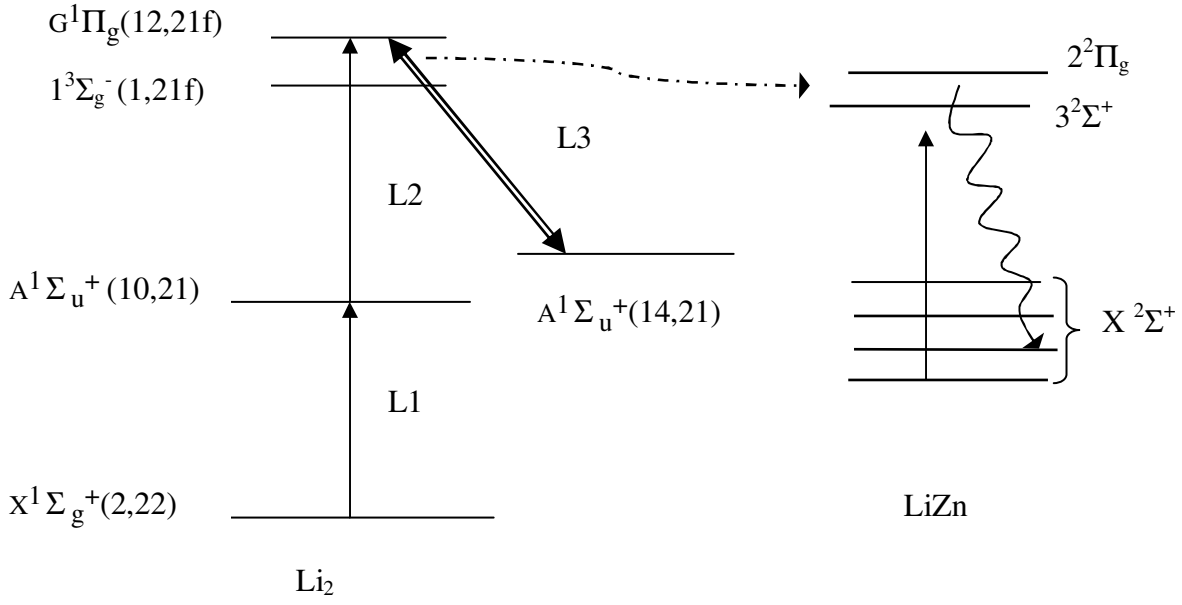

Figure 5.11 Excitation scheme for Li_2 (left) and energy levels in LiZn (right). The mixed levels used in this work are nearly resonant with some levels in the $3^2\Sigma^+$ and $2^2\Pi_g$ states of LiZn, making the perturbed pair a strong candidate to investigate the effect that spin plays in the photochemical reaction $Li_2^*(\ G^1\Pi_g, 1^3\Sigma_g^-) + Zn \rightarrow LiZn^*(3^2\Sigma^+, 2^2\Pi_g) +$ Li(2s).

5.11 Conclusion

In the lithium dimer, we have experimentally demonstrated that the mixing coefficients of a pair of rovibrational levels initially weakly mixed by the spin-orbit interaction may be altered using three optical fields. The extent of this all-optical control of valence electron spin polarization depends on the magnitude of the Rabi frequency of a strong coupling field. When the coupling field is resonant with the predominately singlet state of the mixed pair, an Autler-Townes split pair is created. As one of the singlet-characterized components of the AT pair moves closer in energy to the predominately triplet state, the mixing between the perturbed pair is enhanced. The maximum change in mixing coefficients achieved in our experiment was 112%. This technique has great potential to increase the mixing between other perturbed pairs or even to be used to create mixed pairs from two energy levels that are initially unmixed. Such quantum state character control may also prove to be useful in applications such as the controlling of chemical reaction dynamics or cold molecule formation.

References:

[1] O. Salihoglu, Ph.D. Thesis, Temple University (2009)

[2] G. Lazarov, A. M. Lyyra, and L. Li, J. Mol. Spec. **205**, 73 (2001)

[3] L. Li, T. An, T.-J. Whang, A. M. Lyyra, W. C. Stwalley, R. W. Field, and R. A. Bernheim, J. Chem. Phys. **96**, 3342 (1992)

[4] S. Antonova, Ph.D. Thesis, Temple University (1998)

[5] B. Barakat, R. Bacis, F. Carrot, S. Churassy, P. Crozet, F. Martin, and J. Verges, Chem. Phys. **102**, 215 (1986)

[6] K. Urbanski, S. Antonova, A. Yiannopoulou, A. M. Lyyra, L. Li, and W. C. Stwalley, J. Chem. Phys. **104**, 2813 (1996). See also Errata J. Chem. Phys. **116**, 10557 (2002)

[7] I. Russier, A. Yiannopoulou, P. Crozet, A. J. Ross, F. Martin, and C. Linton, J. Mol. Spec. **184**, 129 (1997)

[8] K. Urbanski, S. Antonova, L. Li, A. M. Lyyra, L. Li, and B. Ji, J. Chem. Phys. **109**, 912 (1998)

[9] A. Yiannopoulou, B. Ji, L. Li, M. Li, K. Urbanski, A. M. Lyyra, W. C. Stwalley, G. –H. Jeung, J. Chem. Phys. **101**, 3581 (1994)

[10] G.-H. Jeung, Private Communication, (2009)

[11] D. R. Skinner., and R.E. Witcher, J. Phys. E, **5**, 237 (1972)

[12] R. J. Le Roy, Level 8.0: A Computer Program for Solving the Radial Schrodinger Equation for Bound and Quasibound Levels, Chemical Physics Research Report No. CP-663, University of Waterloo (2007)

[13] S. Gerstenkorn, and P. Luc, *Atlas du Spectre d'Absorption de la Molecule d'Iode*, CNRS, Orsay, France 1977, 1978

[14] S. Gerstenkorn, and P. Luc, Revue de Physique Applique, **14**, 791 (1979)

[15] W. Demtroder, *Laser Spectroscopy*, Springer-Verlag, Berlin Heidelberg New York (1971)

[16] J. Qi, G. Lazarov, X. Wang, L. Li, L. M. Narducci, A. M. Lyyra, and F. C. Spano, Phys. Rev. Lett. **83**, 288 (1999)

[17] Ergin Ahmed and Teodora Kirova, Private Communication, (2009)

[18] Ergin Ahmed and A. Marjatta Lyyra, Private Communication, (2009)

[19] P.D. Kleiber, A. M. Lyyra, K. M. Sando, V. Zafiropulos, and W. C. Stwalley, J. Chem. Phys. **85** (10) 5493, 1986

References Cited:

Ahmed, E., Hansson, A., Qi, P., Li, L., Kirova, T., Qi, J., Lazoudis, A., Magnier, S., Kotochigova, S., and Lyyra, A. M., J. Chem. Phys. **124**, 084308 –1 to 13 (2006)

Ahmed, E. and Kirova, T., Private Communication, (2009)

Ahmed, E. and Lyyra, A. M., Private Communication, (2009)

Ahmed, E., and Lyyra, A. M., Phys. Rev. A **76**, 053407 (2007)

Ahmed, E., Qi, P., Beser, B., Bai, J., Field, R. W., Huennekens, J. P., and Lyyra, A. M., Phys. Rev. A **77**, 053414, (2008)

Ahmed, E., Qi, P., and Lyyra, A. M., Phys. Rev. A **79**, 062509 (2009)

Allen, L., and Elberly, J. H., *Optical Resonance and Two Level Atoms* (Dover, New York, 1987)

Alzetta, G., Moi, L., and Orriols, G. , Il Nuovo Cimento **52B**, 209 (1979)

Antonova, S. N., Ph.D. Thesis, Temple University (1998)

Arimondo, E., Progress in Optics **35**, 257 (1996)

Arimondo, E. and Orriols, G., Lettere al Nuovo Cimento **17**, 333 (1976)

Autler, S. H., and Townes, C. H., Phys. Rev. **100**, 703 (1955)

Barakat, B., Bacis, R., Carrot, F., Churassy, S., Crozet, P., Martin, F., and Verges, J., Chem. Phys. **102**, 215 (1986)

Berman. P. R., Phys. Rev. A **58**, 4886 (1998)

Bernath, P. F., *Spectra of Atoms and Molecules*, (Oxford University Press, Oxford, 1995)

Bernheim, R. A., Gold, L. P., Kelly, P. B., Tipton, T., and Veirs, D. K., J. Chem. Phys. **74**, 2749 (1981)

Blume, M., Freeman, A. J., and Watson, R. E., Phys Rev. A, **134**, 320 (1964)

Boller, K. J., Imamoglu, A., Harris, S. E., Phys. Rev. Lett. **66**, 2593 (1991)

Borde, C. J., and Hall, J. L., *Laser Spectroscopy*, edited by A. Mooradian and R. G. Brewer (Plenum, New York, 1974)

Born, M., and Oppenheimer, J. R., Ann. Phys., **84**, 457 (1927)

Bouloufa, N., Cacciani, P., Vetter, R., Yiannopoulou, A., Martin, F., and Ross, A. J., J. Chem. Phys. **114**, 8445 (2001)

Brown, J. M., Hougen, J. T., Huber, K. P., Johns, J.W.C., Kopp, I., Lefebvre-Brion, H., Merer, A. J., Ramsey, D. A., Rostas, J., and Zare, R. N., J. Mol. Spec. **55**, 500 (1975)

Budker, D., Kimball, D. F., Rochester, S. M., and Yashchuk, V. V., Phys. Rev. Lett **83**, 1767 (1999)

Cohen-Tannoudji, C., *Amazing Light : a volume dedicated to Charles Hard Townes on his 80th birthday*, ed. by Chiao, R. Y. (Springer, New York, 1996)

Cohen-tannoudji, C., C. R. Acad. Sci. **252**, 394 (1961)

Cohen-Tannoudji, C., and Dupont-Roc, J., Phys. Rev. A **5**, 968 (1972)

Cooper, D. L., Hutson, J. M., and Uzer, T., Chem. Phys. Lett., **86**, 472 (1982)

Danzl, J. G., Haller, E., Gustavsson, M., Mark, M. J., Hart, R., Bouloufa, N., Dulieu, O., Ritsch, H., and Nager, H.-C., Science **321**, 1062 (2008)

DeMille, D., Phys. Rev. Lett. **88**, 067901 (2002)

Demtroder, W., *Laser Spectroscopy*, (Springer-Verlag, Berlin, 1971)

Dupre, D., Jost, R., Lombardi, M., Green, P. G., Abramson, E., and Field, R. W., Chem. Phys. **152**, 293 (1991)

Ficek, Z., and Swain, S., Phys. Rev. A **63**, 063815 (2001)

Gerstenkorn, S., and Luc, P., *Atlas du Spectre d'Absorption de la Molecule d'Iode*, CNRS, Orsay, France 1977, 1978

Gerstenkorn, S., and Luc, P., Revue de Physique Applique, **14**, 791 (1979)

Grabowski, A., Heidemann, R., Löw, R., Stuhler, J., and Pfau, T., Fortschr. Phys. **54**, 765 (2006)

Gray, H. R., Stroud Jr., C. R., Opt. Commun. **25**, 359 (1978)

Gray, H. R., Whitley R. M., and Stroud, C. R., Optics Letters **3**, 218 (1978)

Harris, S. E., Phys. Rev. Lett. **62**, 1033 (1989)

Harris, S. E., Phys. Today **50**, Issue 7, 36 (1997)

Harris, S.E., Field, J. E., and Imamoglu, A., Phys. Rev. Lett. **64**, 1107 (1990)

Hau, L. V., Harris, S. E., Dutton, Z., and Behroozi, C. H., Nature **397**, 594 (1999)

Heisenberg, W., Z. Physik **43**, 172 (1927)

Herzberg, G., *Molecular Spectra and Molecular Structure I, Spectra of Diatomic Molecules*, (D. Van Nostrand Company Inc., Princeton, 1950)

Hessel, M. M., and Vidal, C. R., J. Chem. Phys. **70**, 4439 (1979)

Huennekens, J., Loza, A., Masters, M., and Sando, K. M., J. Chem. Phys. **88**, 6013 (1988)

Huennekens, J., Walker, T. G., and McClain, S. C., J. Chem. Phys. **83**, 4949, 1985

Hund, F., Z. Phys. **42**, 93 (1927)

Hund, F., Z. Phys. **63**, 719 (1930)

Ikram, M., and Zubiary, M. S., Phys. Rev. A **65**, 044305 (2002)

Imamoglu, A. and Harris, S.E., Opt. Lett. **14**, 1344 (1989)

Ivanov, V. S., Sovkov, B. B., Li, L., Lyyra, A. M., Lazarov, G., and Huennekens, J., J. Mol. Spec. **194**, 147 (1999)

Jeng, W.-H., Xie, X., Gold, L. P., and Bernheim, R. A., J. Chem. Phys. **94**, 928 (1991)

Jeung, G.-H., Private Communication, (2009)

Judd, B. R., *Angular Momentum Theory for Diatomic Molecules* (Academic Press, New York, 1975)

Kash, M. M., Sautenkov, V. A., Zibrov, A. S., Hollberg, L., Welch, G. R., Lukin, M. D., Rostovtsev, Y., Fry, E. S., and Scully, M. O., Phys. Rev. Lett. **82**, 5229 (1999)

Kayama, K., and Baird, J. C., J. Chem. Phys., **46**, 2604 (1967)

Kirova, T. V., PhD. Thesis, Temple Univeristy (2005)

Kirova, T. V., Private Communication (2009)

Kirova, T. V., and Spano, F. C., Phys. Rev. A **71**, 063816 (2005)

Kleiber, P.D., Lyyra, A. M., Sando, K. M., Zafiropulos, V., and Stwalley, W. C., J. Chem. Phys. **85** (10) 5493, 1986

Kusch, P., and Hessel, M. M., J. Chem. Phys. **67**, 586 (1977)

Kuznetsova, E., Gacesa, M., Pellegrini, P., Yelin, S. F., and C*ô* té, R., New J. Phys. **11**, 055028 (2009)

Lazarov, G., Ph.D. Thesis, Temple University (2000)

Lazarov, G., Lyyra, A. M., and Li, L., J. Mol. Spec. **205**, 73 (2001)

Lazoudis, A., Ph.D. Thesis, Temple University (2005)

Lazoudis, A., Ahmed, E., Li, L., Kirova, T., Qi, P., Hansson, A., Magnes, J., and Lyyra, A. M., Phys. Rev. A, 7**8,** 043405 (2008)

Lefebvre-Brion, H., and Field, R. W., *Perturbations in the Spectra of Diatomic Molecules* (Academic Press, Orlando, 1986)

Lefebvre-Brion, H., Field, R. W., *The spectra and Dynamics of Diatomic molecules*, (Elsevier Academic Press, 2004)

Le Roy, R. J., Level 8.0: A Computer Program for Solving the Radial Schrodinger Equation for Bound and Quasibound Levels, Chemical Physics Research Report No. CP-663, University of Waterloo (2007)

Li, F-L., Zhu, S-Y., Opt. Commun. **162**, 155 (1999)

Li, L., An, T., Whang, T.-J., Lyyra, A. M., Stwalley, W. C., Field, R. W., and Bernheim, R. A., J. Chem. Phys. **96**, 3342 (1992)

Li, L., Antonova, S., Yiannopoulou, A., Urbanski, K., and Lyyra, A. M., J. Chem. Phys. **105**, 9859 (1996)

Li, L., Field, R. W., J. Phys. Chem., **87,** 3020 (1983)

Li, L., Field, R. W., J. Mol. Spec. **117**, 245 (1986)

Li, L., Field, R. W., J. Mol. Spec. **123**, 237 (1987)

Li, L., and Lyyra, A. M., Spectrochimica Acta Part A, **55**, 2147 (1999)

Li, L., Qi, P., Lazoudis, A., Ahmed, E., and Lyyra, A. M., Chem. Phys. Lett. **403**, 262 (2005)

Li, L., Yiannopoulou, A., Urbanski, K., Lyyra, A. M., Ji, B., Stwalley, W. C., and An, T., J. Chem. Phys. **105**, 6192 (1996)

Li, L., Zhu, Q., and Field, R. W., J. Mol. Spec. **134**, 50 (1989)

Li, L., Zhu, Q., Lyyra, A. M., Whang, T. –J., Stwalley, W. C., Field, R. W., and Alexander, M. H., J. Chem. Phys. **97**, 8836 (1992)

Linton, C., Martin, F., Ross, A. J., Russier, I., Crozet, P., Yiannopoulou, A., Li, L., and Lyyra, A. M., J. Mol. Spec. **196**, 20 (1999)

Lyyra, A. M., Qi, J., and Spano, F. C., Herzberg Memorial Issue of the Canadian Journal of Physics **79**, 547 (2001)

Lyyra, A. M., Spano, F. C., Qi, J., and Kirova, T., ACS Symposium Series Vol. **821** on Laser Control and Manipulation of Molecules**,** 304 **(**2002)

Masters, M., Huennekens, J., Luh, W. T., Li, L., Lyyra, A. M., Sando, K., Zafiropulos, V., and Stwalley, W. C., J. Chem. Phys. **92**, 5801 (1990)

Merzbacher, E., *Quantum Mechanics*, 3rd edition, (John Wiley and Sons Inc., Hoboken NJ USA, 1998)

Meystre, P., and Sargent III, M., *Elements of quantum Optics* (Springer-Verlag, Berlin, 1991)

Minogin, V. G., and Rozhdestvenskii, Y.V., Opt. Commun. **64**, 172 (1987)

Morgus, L., Ph.D. Thesis, Lehigh University (2005)

Motohiro, S., Nakajima, S., and Ishiwata, T., J. Chem. Phys. 117, 187 (2002)

Ni, K. –K., Ospelkaus, S., de Miranda, M. H. G., Pe'er, A., Neyenhuis, B., Zirbel, J. J., Kotochigova, S., Julienne, P. S., Jin, D. S., Ye, J., Science **322**, 231 (2008)

O'Calligan, M. J., and Cooper, J., Phys. Rev. A. **39**, 6206 (1989)

O'Calligan, M. J., and Gallagher, A., Phys. Rev. A. **39**, 6190 (1989)

Pashov, A., Jastrzebski, W., and Kowalczyk, P., J. Chem. Phys. **113**, 6624 (2000)

Poteau, R., and Spiegelmann, F., J. Mol. Spec. **171**, 299 (1995)

Qi, P., Lazarov, G., and Lyyra, A. M., J. Mol. Spec. **247**, 184 (2008)

Qi, J., Lazarov, G., Wang, X., Li, L., Narducci, L. M., Lyyra, A. M., and Spano, F. C., Phys. Rev. Lett. **83,** 288 (1999)

Qi, J., and Lyyra, A. M., Phys. Rev. A **73**, 043810 (2006)

Qi, J., Spano, F. C., Kirova, T., Lazoudis, A., Magnes, J., Li, L., Narducci, L. M., Field, R. W., and Lyyra, A. M., Phys. Rev. Lett**. 88**, 173003 (2002)

Quesada, M. A., Lau, A. M. F., Parker, D. H., and Chandler, D. W., Phys. Rev. A **36**, 4107 (1987)

Renzoni, F., Lindner, A., and Arimondo, E., Phys. Rev. A **60**, 450 (1999)

Russier, I., Yiannopoulou, A., Crozet, P., Ross, A. J., Martin, F., and Linton, C., J. Mol. Spec. **184**, 129 (1997)

Sagle, J., Namiotka, R. K., Huennekens, J., J. Phys. B **29**, 2629 (1996)

Salihoglu, O., PhD. Thesis, Temple University (2009)

Salihoglu, O., Qi, P., Ahmed, E., Kotochigova, S., Magnier, S., and Lyyra**,** A. M., J. Chem. Phys. **129**, 174301 (2008)

Scully, M. O., and Fleischhauer, M., Phys. Rev. Lett. 69, 1360 (1992)

Scully, M. O., Zhu, S. Y., and Gavrielides, A., Phys. Rev. Lett **62**, 2813 (1989)

Scully, M.O. and Zubairy, M.S., *Quantum Optics*, (Cambridge University Press, Cambridge, 2002)

Sha, G., He, J., Jiang, B., and Zhang, C., J. Chem. Phys. **102**, 2772 (1995)

Shapiro, M., and Brumer, P., *Principles of the Quantum Control of Molecular Processes*, (Wiley-VCH, Hoboken, 2003)

Sild, O., Rozman, M., and Hizhnyakov, V., Opt. Commun. **53**, 173 (1985)

Skinner, D. R.,and Witcher, R.E., J. Phys. E, **5**, 237 (1972)

Soorkia, S., Le Quéré, F., Léonard, C., and Figgen, D., Molecular Physics **105**, 1095 (2007)

Spano, F. C., J. Chem. Phys. **114**, 276 (2001)

Stenholm, S., *Foundations of laser spectroscopy*, (Wiley-Interscience, New York , 1984)

Steinfeld, J. I., *Molecules and Radiation: an Introduction to Modern Molecular Spectroscopy* (Dover, New York, 1985)

Sun, H., and Huennekens, J., J. Chem. Phys., **97**, 4714 (1992)

Sun, Z., and Nanquan, L., Phys. Rev. Lett. **91**, 023002 (2003)

Sussman, B. J., Townsend, D., Ivanov, M. Y., Stolow, A., Science **314**, 278 (2006)

Sweeney, S. J., Ahmed, E., Qi, P., Kirova, T., Lyyra, A. M., and Huennekens, J., J. Chem. Phys. **129,** 154303 (2008)

Tellinghuisen, J., *Photodissociation and Photoionization*, edited by K. P. Lawley, (Wiley, New York, 1985)

Urbanski, K., Antonova, S., Lyyra, A. M., L. Li, and Ji, B., J. Chem. Phys. **109**, 912 (1998)

Urbanski, K., Antonova, S., Yiannopoulou, A., Lyyra, A. M., Li, L., and Stwalley, W. C., J. Chem. Phys. **104**, 2813 (1996). See also Errata J. Chem. Phys. **116**, 10557 (2002)

Vasilenko, L. S., Chebotayev, V. P., and Shishaev, A. V., JETP Lett. **12**, 113 (1970)

Veseth, L., Theo. Chim. Acta, **18**, 368 (1970)

Viteau, M., Chotia, A., Allegrini, M., Bouloufa, N., Dulieu, O., Comparat, D., and Pillet, P., Science **321**, 232 (2008)

Wang, X. J., Magnes, J., Lyyra, A. M., Ross, A. J., Martin, F., Dove, P. M., and Le Roy, R. J., J. Chem. Phys. **117**, 9339 (2002)

Wang, X. J., Yang, J., Qi, J. B., and Lyyra, A. M., J. Mol. Spec. **191**, 295 (1998)

Whang, T. J., Lyyra, A. M., Stwalley, W. C., and Li, L., J. Mol. Spec. **149**, 505 (1991)

Xie, X., and Field, R. W., Chem. Phys. **99**, 337 (1985)

Xu, J., and Hu, X. M., Chin. Phys. Lett. **24**, 933 (2007)

Yi, P., Ji, B., Cheung, A. S.-C., Stwalley, W. C., Field, R. W., Lyyra, A. M., and Li, L., Chem. Phys. Lett. **349**, 426 (2002)

Yi, P., Song, M., Liu, Y., Field, R. W., Li, L., and Lyyra, A. M., Optics Comm. **233** (1-3): 131 (2004)

Yiannopoulou, A., Ph.D. Thesis, Temple University (1995)

Yiannopoulou, A., Ji, B., Li, L., Li, M., Urbanski, K., Lyyra, A. M., Stwalley, W. C., and Jeung, G.-H., J. Chem. Phys. **101**, 3581 (1994)

Yiannopoulou, A., Urbanski, K., Antonova, S., Lyyra, A. M., Li, L., An, T., Whang, T. J., Ji, B., Wang, X. T., Stwalley, W. C., Leininger, T., and Jeung, G.-H., J. Chem. Phys. **103**, 5898 (1995)

Zare, R. N., *Angular Momentum*, Wiley-Interscience, New York, 1986

Zare, R. N., *Angular Momentum: Understanding Spatial Aspects in Chemistry and Physics* (Wiley, New York, 1988)

Zibrov, A. S, Lukin, M. D., Hollberg, L., Nikonov, D. E., Scully, M. O., Robinson, H. G., and Velichansky, V. L., Phys. Rev. Lett. **76**, 3935 (1996)

Zibrov, A. S., Lukin, M. D., Nikonov, D. E., Hollberg, L., Scully, M. O., Velichansky, V. L., and Robinson, H. G., Phys. Rev. Lett **75**, 1499 (1995)